TYROSINE-BASED SCHIFF BASE LIGANDS AND THEIR Zn(II) AND Cd(II) COMPLEXES AS FLUOROGENIC CHEMOSENSORS FOR ANIONS

Nitish Kumar

A dissertation submitted for the partial fulfillment of B.S.-M.S. Dual Degree in Science

Indian Institute of Science Education and Research Mohali

April 2015

Certificate of Examination

This is to certify that the dissertation titled "Tyrosine-based Schiff base ligands and their Zn(II) and Cd(II) complexes as fluorogenic chemosensors for anions" submitted by Mr. Nitish Kumar (Reg. No. MS10088) for the partial fulfillment of BS-MS dual degree programme of the Institute has been examined by the thesis committee members duly appointed by the Institute. The committee finds the work done by the candidate satisfactory and recommends that the thesis be accepted.

Prof. Ramesh Kapoor	Dr. Ramesh Ramachandran	Prof. Sanjay Mandal
(Member)	(Member)	(Convener & Supervisor)

Dated: April 24, 2015

Declaration

The work presented in this dissertation has been carried out by me under the guidance of Prof. Sanjay Mandal at the Indian Institute of Science Education and Research Mohali. This work has not been submitted in part or in full for a degree, a diploma, or a fellowship to any other university or institute. Whenever contributions of others are involved, every effort is made to indicate this clearly, with due acknowledgement of collaborative research and discussions. This thesis is a bona fide record of original work done by me and all sources listed within have been detailed in the bibliography.

Nitish Kumar

Dated: April 24, 2015

In my capacity as the supervisor of the candidate's project work, I certify that the above statements by the candidate are true to the best of my knowledge.

Prof. Sanjay Mandal

Dated: April 24, 2015

Acknowledgements

I would like to thank my supervisor Prof. Sanjay Mandal for providing me an opportunity to work with him and for his guidance throughout the project. I am also very thankful to Navnita Kumar. She was always there to help me with her valuable comments whenever I faced problem.

I would also like to thank my lab mates Biswajit, Sandeep, Vijay, Gouri, Datta, Prasenjit, Gaurav, Shradha for their support and help. I would like to thank IISER, Mohali for providing with all the facilities for this project work and also to MHRD, Govt. of India for providing an Inspire fellowship.

Finally, I would like to thank all of my friends, family and my parents, and God.

List of Figures

List of Schemes

List of Tables

Contents

Abstract

In this work, three new chiral ligands based on L-tyrosine, namely L-N-(methyl-3-nitro)-Tyrosine [L-H_2Tyr-3-nitro], L-N-(methyl-3-chloro)-Tyrosine [L-H_2Tyr-3-chloro] and L-N-(methyl-3-methoxy)-Tyrosine [L-H_2Tyr-3-methoxy], and their Zn(II) and Cd(II) complexes are prepared in excellent yields. The purity of the ligands is confirmed by ^{1}H NMR spectroscopy and melting point data. The ligands are characterized further by FT-IR, Fluorescence and UV-Vis spectroscopy, powder X-ray diffraction, and ESI-MS analysis. On the other hand, an extensive structural characterization of the metal complexes is done by elemental analysis, FT-IR and Fluorescence spectroscopy, powder X-ray diffraction. The chirality of ligands and metal complexes is established in the solution state by polarimetry. Utilizing the fluorescence property of both ligands and the metal complexes, these are examined for their sensing ability for various analytes, such as KF, KCl, KBr, KI and NaOAc, which play vital roles in many chemical, physiological and industrial processes. The differential behavior of the ligands based on the solvent polarity is also studied. These are found to be excellent fluorogenic chemosensors for fluoride and iodide ions.

Chapter I

Introduction

Luminescent materials have been in use for centuries - initially for decorative purposes and later on in fluorescent tubes and lamps, optical brighteners, plasma screens, fluorescent and phosphorescent paints, phosphorescent labels, safety signs.[1] However, in recent past, the high sensitivity and selectivity of the fluorescence spectroscopy has opened new avenues for their use as chemo- and biosensors.[2] A tremendous up-rise in the synthesis and modulation of sensors has been observed due to their immense importance in national security and environmental hazards. In the literature, many diverse fluorogenic sensors have been reported for detection of analytes like various cations (Pb^{2+}, Hg^{2+}, etc.), anions (F^-, PO_4^{3-}, etc.) and small neutral molecules (nitrobenzene, aniline, etc.).[3]

Luminescence is the phenomenon of the emission of light arising from excited electronic states following absorption of light. Depending on the nature of the excited state, luminescence can be divided into two categories: fluorescence and phosphorescence. Fluorescence is spin-allowed and has typical lifetimes in the order of nanoseconds; whereas, phosphorescence is spin-forbidden and lifetimes can be of the order of several seconds.[4] This phenomenon is described by the Jablonski diagram shown in Figure 1.

Luminescent compounds consist usually of organic chromophores with conjugated π-backbones and little spin-orbit coupling. Hence, the selection rules are determined by the symmetry of the singlet ground and excited states. The strongest emission is usually from the lowest excited singlet state to the singlet ground state and such transitions are either $\pi - \pi*$ or $n - \pi^*$ in nature. Amino acids like tyrosine, phenylalanine and tryptophan with their natural luminescence ability, not only serve as good candidates for this purpose but also open a new dimension in the area of enantioselective sensing. The introduction of d^{10} metal ions into these systems can further enhance their luminescence property by providing structural rigidity to the organic ligands and blocking the non-radiative pathway for emissions.

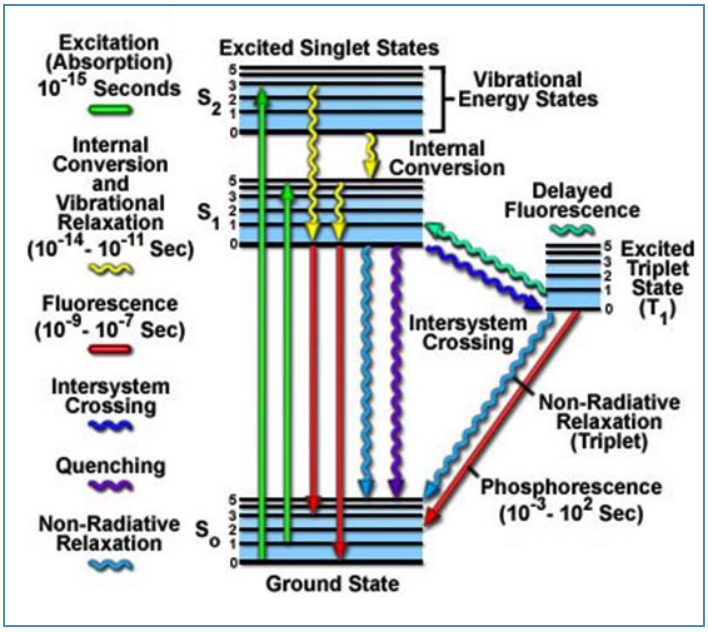

Figure 1. Schematic drawing of the Jablonski diagram.

This spatial arrangement of chromophores with d^{10} metal ions provides better luminescence properties attributing to various effects like metal to ligand charge transfer (MLCT), ligand to metal charge transfer (LMCT), ligand to ligand charge transfer (LLCT) and metal to metal charge transfer (MMCT) as depicted in Figure 2.

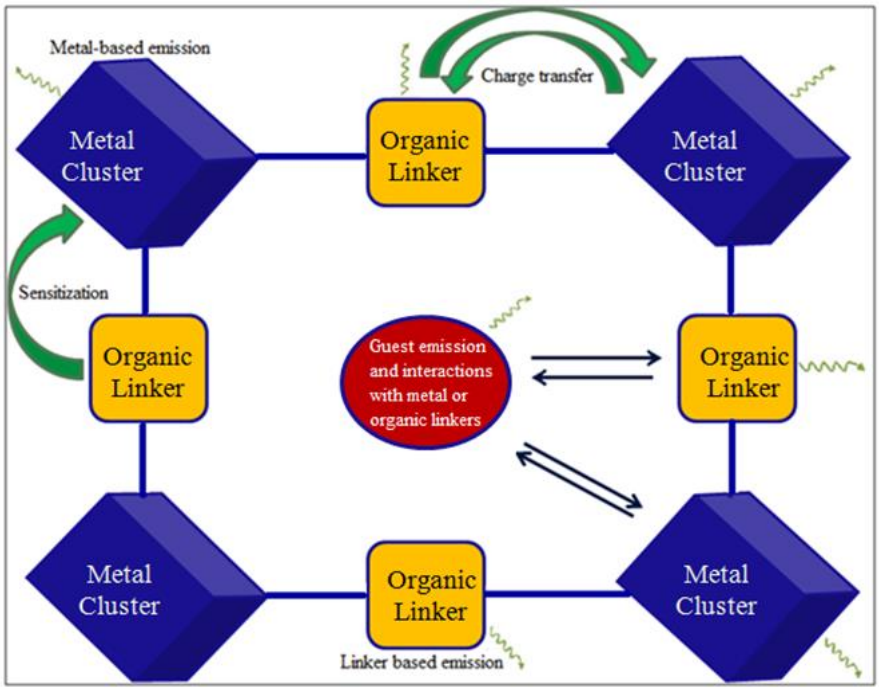

Figure 2. Representation of various emission possibilities (Adapted from Reference 5).

Ligand-to-metal charge transfer (LMCT) is an electronic transition in a metal complex that corresponds to the excitation populating an electronic state in which considerable electron transfer from a ligand to a metal centre has occurred. The organic ligands possess σ, σ*, π, π*, and nonbonding (n) molecular orbitals. If the ligand molecular orbitals are full, charge transfer may occur from the ligand molecular orbitals to the empty or partially filled metal d-orbitals (Figure 3).[6] LMCT transitions result in intense bands. Forbidden d-d transitions may also take place giving rise to weak absorptions. Ligand to metal charge transfer results in the reduction of the metal. These are common for coordination compounds having π-acceptor ligands. Since d^{10} metals have completely filled d shells, LMCT transitions must terminate at the next higher s orbital of the metal. Generally, d^{10} complexes are colorless because their LMCT absorptions appear in the UV region.

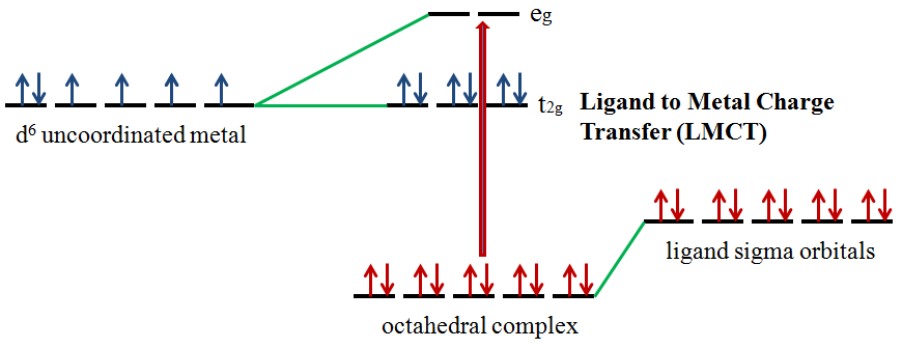

Figure 3. Schematic representation of the orbitals for a Ligand to Metal Charge Transfer (LMCT) complex.

Metal-to-ligand charge transfer (MLCT) transitions may occur if the metal is in a low oxidation state (electron rich) and the ligand possesses low-lying empty orbitals. Upon the absorption of light, electrons in the metal orbitals are excited to the ligand π* orbitals (Figure 4).[6] MLCT transitions result in intense bands. Forbidden d–d transitions may also occur. This transition results in the oxidation of the metal.

Metal-to-metal charge transfer (MMCT) is an electronic transition of a bi- or polynuclear metal complex that corresponds to the excitation populating an electronic state in which considerable electron transfer between two metal centres has occurred.[7]

Ligand-to-ligand charge transfer (LLCT) is an electronic transition of a metal complex that corresponds to the excitation populating an electronic state in which considerable electron transfer between two ligands has occurred.[7]

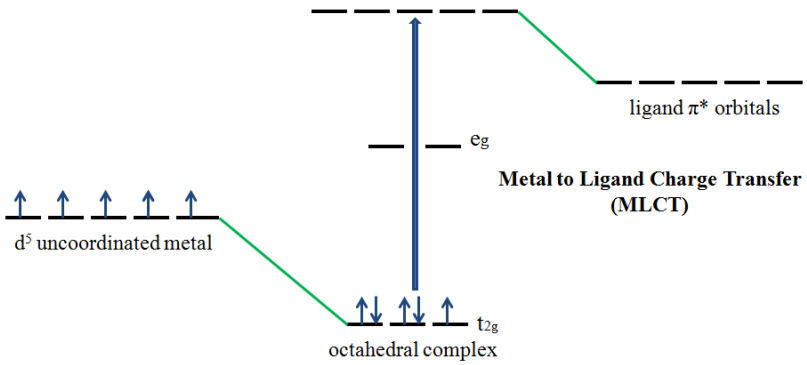

Figure 4. Schematic representation of the orbitals for a Metal to Ligand Charge Transfer (MLCT) complex.

In some cases, even more than one effect comes into play, hence the overall emission depends on the coordination architecture of these complexes. As mentioned earlier, the enhanced luminescence property is further employed in sensing various analytes, especially anions. Anions play a major role in our daily life, being crucial to many physiological functions as well as various industrial processes. Consequently, in the environment anionic species can be either essential to sustain growth or act as harmful pollutants. Thus, the development of colorimetric and luminescent sensors for anions has become a very active area of research. In this study, the function, concentration and location of the negatively charged species are monitored.[8] Neutral macrocycles are the most common anion sensors in the literature[9] where anion-π interactions are monitored. Homochiral amino acid based luminescent sensors are being considered as a better alternative over the macrocycles due to their ease of synthesis and cost effectiveness.[10]

Anion–π interaction is a novel type of non-covalent forces between electron deficient aromatic systems and anions.[11] Due to the counterintuitive nature (anions are expected to exhibit repulsive interactions with aromatic π-systems due to their electron donating character) and the chemically challenging factors inherent to the nature of anions (larger size and much higher free energies of solvation compared to cations, wide range of coordination geometries and electronic saturation), these anion–π interactions were previously not considered relevant. However, the recent theoretical and experimental investigations have established the importance of anion–π

interactions in many key chemical and biological processes.[12] On the basis of these anion–π interactions, highly selective anion receptors have been designed for effectively accomplishing various functions of prime environmental or biological importance. The bond energies for such anion–π supramolecular pairs are in the range 20–70 kJ/mol. This unfavorable interaction with a negative π-surface can become attractive for aromatic moieties with electron-withdrawing substituents like nitro, fluoro or N-heterocyclic rings. Extensive studies have shown that in general, the electrostatic and anion-induced polarization contributions dominate anion–π interactions, but recently an alternate driving force was proposed for substituted benzene rings.[13] Aromatic rings with large positive quadrupole moments establish strong anion–π interactions. Anion-induced polarization arises from the interaction of the anion with the π-system induced dipole and has significant contributions for molecules with high polarizability or extended π-systems.

Depending on the anion and the π-system types, three interaction modes are possible between a π-acidic aromatic ring and an anion located above it: (a) non-covalent anion–π contact with the anion centered or displaced from the ring centroid, (b) anion-donor–π-acceptor interaction with positioning of the anion over the π-system periphery and (c) strongly covalent σ interaction (Figure 5).

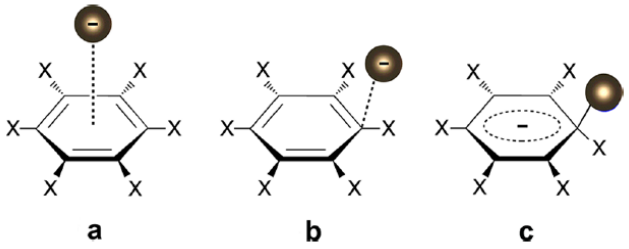

Figure 5. Anion interaction types with π-systems (a) anion–π, (b) anion-donor-π-acceptor, and (c) strongly covalent σ interaction (Adapted from reference 13).

These interactions can be monitored by various changes in the spectral responses to the analyte in the fluorescence spectra of the sensor. On interaction with the analyte, a sensor can show modulation in the intensity, excitation spectrum, emission spectrum, anisotropy, or lifetime of the sensing probe (Figure 6). The most direct sensing method is when the fluorescence intensity of the probe changes in response to the analyte. This change can be either quenching or enhancement in the intensity.[4]

Solvent polarity and the local environment around the fluorophore (sensor) have a drastic effect on the emission spectra. Emission from fluorophores generally occurs at wavelengths that are longer than those at which absorption occurs. Solvent effects shift the emission to lower energy due to stabilization of the excited state by the polar solvent molecules. Typically, the fluorophore has a larger dipole moment in the excited state compared to the ground state. After excitation, the solvent dipoles can reorient or relax around the fluorophore dipole, which lowers the energy of the excited state. As the solvent polarity is increased, this effect becomes larger, resulting in emission at lower energies or longer wavelengths. Generally, polar fluorophores display a large sensitivity to the solvent polarity. Nonpolar molecules are much less sensitive to solvent polarity, for example, unsubstituted aromatic hydrocarbons.[4]

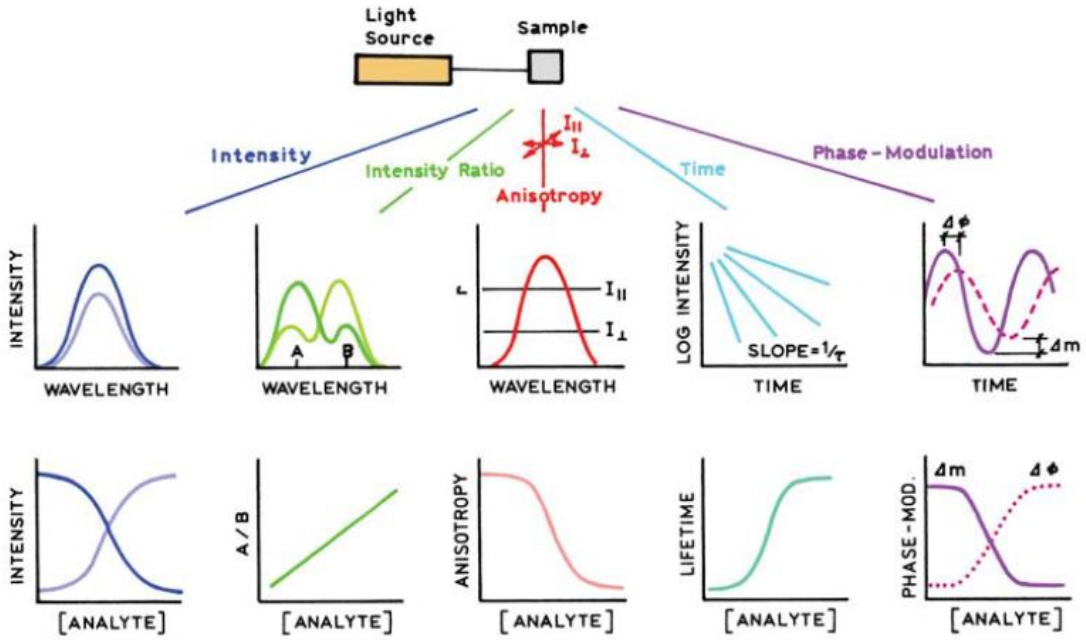

Figure 6. Spectral observables for fluorescence sensing. From left to right, sensing is performed using intensities, intensity ratios, anisotropies, time-domain lifetimes, and phase-modulation measurements. (Adapted from Reference 4).

Present work

This thesis focuses on the synthesis, structural characterization and sensing abilities of three new L-tyrosine based reduced Schiff base ligands as shown in Figure 7 and their Zn(II) and Cd(II) complexes. The purity of the ligands is confirmed by ^{1}H NMR spectroscopy. Further, the ligands and the metal complexes are characterized thoroughly by elemental analysis, FT-IR,

Fluorescence and UV-Vis spectroscopy, powder X-ray diffraction, and ESI-MS analysis. The chirality of these compounds is established in the solution state by polarimetry.

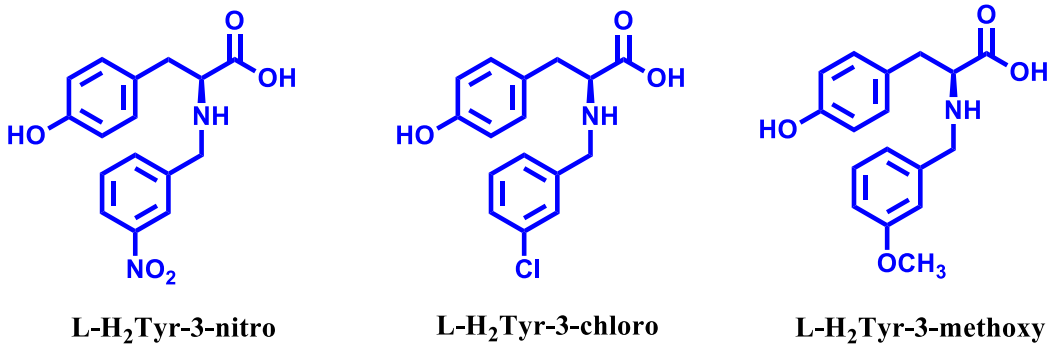

Figure 7. New ligands synthesized for this study.

L-tyrosine is a natural fluorophore and chiral in nature. It has two different emission wavelengths at 220 nm and 270 nm due to the presence of two different functional groups, one phenolic and the other carboxylate. The d^{10} metal complexes of these L-tyrosine based ligands can further help in enhancing the fluorescence property. The effect of substitution of a proton of amine moiety in L-Tyrosine with 3-nitrobenzyl, 3-chlorobenzyl and 3-methoxybenzyl groups on fluorescence behaviour is well explored. The sensing behavior of the nitro derivative is compared with its chloro and methoxy analogues. Hence, both ligands and the metal complexes are examined for their sensing ability for various analytes, such as KF, KCl, KBr, KI and NaOAc. The differential behavior of these sensors based on the solvent polarity is also studied.

Chapter II

Experimental Section

Materials and Methods

All required chemicals and solvents were obtained from commercial sources and used as received without any further purification. FTIR spectra were collected for compounds prepared as KBr pellets using Perkin Elmer Spectrum RX I FT-IR spectrometer in the 400-4000 cm^{-1} range. Elemental analysis (C, H, N) was carried out using a Leco-USA Tru Spec CHNS micro version 2.7x analyser. UV-Vis spectra were recorded on Agilent technologies Cary 5000 UV-Vis-NIR Spectrophotometer for the range 200-800 nm. Solution state fluorescence spectra were recorded on RF-5301 PC Spectroflurophotometer from Shimadzu. ^1H NMR spectra of the sodium salt of the ligands were obtained in D_2O at 25 °C on a Bruker ARX-400 spectrometer. Melting point was measured on Buchi M-565 melting point apparatus. Powder X-ray diffraction studies were carried on a Rigaku Ultima IV diffractometer, ESI mass spectrometry was performed using either Waters HRMS instrument or Thermo Scientific LTQ XL LC-MS instrument for the 50-2000 amu range located in the X-ray facility of IISER Mohali.

Synthesis of Ligands

L-N-(methyl-3-nitro)-Tyrosine [L-H_2Tyr-3-nitro]. To a solution of 250 mg of L-tyrosine (1.38 mmol) and 110 mg of NaOH (2.75 mmol) in 7 mL of a methanol: water mixture (v/v 1:1) was added 209 mg of 3-nitrobenzaldehyde (1.38 mmol). The resulting solution was stirred for 24 hours. To this solution, 53 mg of $NaBH_4$ (1.4 mmol) was added at 0 °C and the contents stirred until the yellow color disappeared. The pH of the solution was adjusted to 5 using (~2 mL) glacial acetic acid and stirred for half an hour. The orange precipitate obtained was filtered off, washed with water and air dried. Yield: 359 mg (82 %). Melting point: 249 ^oC. FTIR (KBr, cm^{-1}): 3419, 3183, 2923, 1607, 1525, 1356, 1247. MS (ESI-TOF): m/z calcd for [(L-H_2Tyr-3-nitro)H]+, 317.1137; found, 317.1091. Specific rotation $[\alpha]^D_{20}$ = 8.00 (0.025 %, water).

L-N-(methyl-3-chloro)-Tyrosine [L-H_2Tyr-3-chloro]. It was prepared following the same procedure as for L-H_2Tyr-3-nitro, replacing 3-nitrobenzaldehyde with 0.16 ml of 3-chlorobenzaldehyde (1.38 mmol) and refluxing the reaction mixture for 5 hours at 80-85 ^oC. The yellow precipitate obtained was filtered off, washed with water and air dried. Yield: 362 mg (86 %). Melting point: 236 ^oC. FTIR (KBr, cm^{-1}): 3410, 3183, 1580, 1396, 1172. MS (ESI-TOF): m/z calcd. for [(L-H_2Tyr-3-chloro)H]+, 306.0897; found, 306.0844. Specific rotation $[\alpha]^D_{20}$ = 40.00 (0.025%, water).

L-N-(methyl-3-methoxy)-Tyrosine [L-H_2Tyr-3-methoxy]. This was also prepared following the same procedure as described for L-H_2Tyr-3-nitro, replacing 3-nitrobenzaldehyde with 0.17 ml of 3-methoxybenzaldehyde (1.38 mmol) and refluxing the reaction mixtue for 6 hours at 80-85 ^oC. Yield: 353 mg (80 %). Melting point: 230 ^oC. FTIR (KBr, cm^{-1}): 3422, 3178, 1591, 1517, 1397, 1261. MS (ESI-TOF): m/z calcd. for [(L-H_2Tyr-3-methoxy)H]+, 302.1392; found, 302.1407. Specific rotation $[\alpha]^D_{20}$ = 48.00 (0.025%, water).

Synthesis of Metal Complexes

[Zn(L-HTyr-3-nitro)$_2$(H_2O)] (1·4H_2O). In a 10 mL round bottom (RB) flask, 25 mg of L-H_2Tyr-3-nitro (0.080 mmol) and 3.8 mg of NaOH (0.092 mmol) were dissolved in 2 mL water. To this was added 11.5 mg of $ZnSO_4.7H_2O$ (0.041 mmol) with stirring. The reaction mixture turned white and was stirred for 24 h. The precipitate obtained was filtered off, washed with water and air dried to obtain a creamy white solid. Yield: 20 mg (78 %). FTIR (KBr, cm^{-1}): 3449, 3261, 3183, 2923, 1598, 1525, 1350, 1247. Anal. Calcd. (%) for $C_{32}H_{40}N_4O_{15}Zn$ (MW 785.5): Calc. C, 48.91; H, 5.09; N, 7.13. Found: C, 48.62; H, 4.01; N, 6.44.

[Cd(L-HTyr-3-nitro)$_2$(H_2O)] (2·3H_2O). In a 10 mL round bottom (RB) flask, 25 mg of L-H_2Tyr-3-nitro (0.080 mmol) and 3.8 mg of NaOH (0.092 mmol) were dissolved in 2 mL water. To this was added 11 mg of $Cd(OAc)_2·2H_2O$ (0.041 mmol) with stirring. The reaction mixture turned white and was stirred for 24 h. The precipitate obtained was filtered off, washed with water and air dried. A creamy white solid was obtained. Yield: 23 mg (86 %). FTIR (KBr, cm^{-1}): 3421, 3261, 3178, 2923, 1585, 1525, 1352, 1247. Anal. Calcd. (%) for $C_{32}H_{38}N_4O_{14}Cd$ (MW 796): Calc. C, 48.24; H, 4.52; N, 7.03. Found: C, 48.25; H, 4.56; N, 7.07.

[Zn(L-HTyr-3-chloro)$_2$(H$_2$O)] (3·2H$_2$O). This was synthesized following the same procedure as for **1** taking 25 mg of L-H$_2$Tyr-3-chloro (0.080 mmol) as the ligand. A creamy white solid was obtained. Yield: 17 mg (65 %), FTIR (KBr, cm^{-1}): 3397, 3275, 2927, 1599, 1515, 1395, 1171. Anal. Calcd. (%) for $C_{32}H_{36}N_2O_9Cl_2Zn$ (MW 728.5): Calc. C, 52.74; H, 4.94; N, 3.84. Found: C, 52.88; H, 5.05; N, 3.33.

[Cd(L-HTyr-3-chloro)$_2$(H$_2$O)] (4·2H$_2$O). This was synthesized following the same procedure as for **2** taking 25 mg of L-H$_2$Tyr-3-chloro (0.080 mmol) as the ligand. A creamy white solid was obtained. Yield: 21mg (80 %), FTIR (KBr, cm^{-1}): 3393, 3275, 2931, 1587, 1515, 1396, 1173. Anal. Calcd. (%) for $C_{32}H_{50}N_2O_{16}Cl_2Cd$ (MW 775): Calc. C, 49.54.48; H, 4.64; N, 3.61. Found: C, 49.25; H, 5.11; N, 3.01.

[Zn(L-HTyr-3-methoxy)$_2$(H$_2$O)] (5·3H$_2$O). This was synthesized following the same procedure as for **1** taking 25 mg of L-H$_2$Tyr-3-methoxy (0.080 mmol) as the ligand. A creamy white solid was obtained. Yield: 13 mg (50 %). FTIR (KBr, cm^{-1}): 3397, 3178, 2958, 1596, 1513, 1397, 1261, 1158. Anal. Calcd. (%) for $C_{34}H_{44}N_2O_{12}Zn$ (MW 737.5): Calc. C, 55.35; H, 5.97; N, 3.79. Found: C, 55.79; H, 6.32; N, 3.30.

[Cd(L-HTyr-3-methoxy)$_2$(H$_2$O)] (6·2H$_2$O). This was synthesized following the same procedure as for **2** taking 25 mg of L-H$_2$Tyr-3-methoxy (0.080 mmol) as the ligand. A creamy white solid was obtained. Yield: 21 mg (78 %). FTIR (KBr, cm^{-1}): 3422, 3274, 2931, 1589, 1516, 1386, 1262, 1171. Anal. Calcd. (%) for $C_{34}H_{42}N_2O_{11}Cd$ (MW 766): Calc. C, 53.26; H, 5.48; N, 3.64. Found: C, 52.88; H, 5.05; N, 3.33.

Powder X-ray Diffraction Studies

PXRD data were recorded on a Rigaku Ultima IV diffractometer equipped with a 3 KW sealed tube Cu KαX-ray radiation (generator power settings: 40 kV and 40 mA) and a DTex Ultra detector using parallel beam geometry (2.5° primary and secondary solar slits, 0.5° divergence slit with 10 mm height limit slit). Each sample grounded into a fine powder using a mortar and a pestle was placed on a glass sample holder that was placed on the sample rotation stage (120 rpm) attachment. The data were collected over an angle range 5° to 50° with a scanning speed of 2° per minute with 0.02° step with XRF reduction for the metal complexes.

Solution State Fluorescence Spectroscopy

The solution state fluorescence spectra were recorded for both the ligands and the metal complexes. In the case of ligands, the solutions were made: (a) in methanol by dissolving them as sodium salts, and (b) in DMSO. Due to the solubility constraint of the metal complexes (these were soluble only in DMSO), their fluorescence spectra were recorded only in DMSO.

Anion sensing studies. The fluorescence property of the ligands and the metal complexes was further utilized for sensing various anions. Three ligands (L-H_2Tyr-3-nitro, L-H_2Tyr-3-chloro and L-H_2Tyr-3-methoxy) and six metal complexes (**1**-**6**) were studied for their sensing ability towards five different analytes: KF, KCl, KBr, KI and NaOAc.

To carry out the sensing studies, 12.6 µL of a 0.1 mM solution of the analyte was added to 2 mL of a 0.6 mM solution of the sensor (ligand or metal complex).

Chapter III

Results and Discussion

The aim of the present work is to generate chiral, luminescent ligands and their metal complexes for sensing of anions. Since it is known that L-tyrosine is a natural fluorophore due to the presence of phenolic group and the carboxylate group, the luminescent behavior of the ligands and their metal complexes is also expected. Furthermore, Zn^{2+} and Cd^{2+} with d^{10} electronic configuration also help in enhancing their luminescence property. Thus, three new chiral ligands, such as L-H_2Tyr-3-nitro, L-H_2Tyr-3-chloro and L-H_2Tyr-3-methoxy, were synthesized by reacting L-tyrosine with 3-nitrobenzaldehyde, 3-chlorobenzaldehyde and 3-methoxybenzaldehyde, respectively, followed by the reduction with sodium borohydride. Using these three ligands, six metal complexes were made with $ZnSO_4{\cdot}7H_2O$ and $Cd(OAc)_2{\cdot}2H_2O$ as the metal salts. General strategies for the synthesis of ligands and the metal complexes are shown in Scheme 1 and Scheme 2, respectively.

Both the ligands and their Zn(II) and Cd(II) complexes were characterized by a number of analytical methods as described below.

^{1}H NMR Spectroscopy

The ^{1}H NMR spectra of L-H_2Tyr-3-nitro, L-H_2Tyr-3-chloro and L-H_2Tyr-3-methoxy ligands are shown in Figures 8-10, respectively.

For L-H_2Tyr-3-nitro, the aromatic region has 8 H of five types in the aromatic region. 2 H at 8.0 ppm and 1 H each at 7.5 and 7.4 ppm correspond to the phenyl ring containing the nitro group. Due to the presence of electron withdrawing group (nitro) these are observed at more downfield. At 6.7 and 6.4 ppm, 2 H each are observed for the phenolic group of tyrosine. In the non-aromatic region, a total five protons of four different types are observed. Two protons of the -CH_2 group of the phenyl moiety are split due to the presence of diastereomers (1 H at 3.5 ppm and 1 H at 3.7 ppm). The proton of the -CH group of chiral carbon centre is observed at 3.2 and the two protons of the -CH_2 group attached with phenolic group of tyrosine appear at 2.7 ppm.

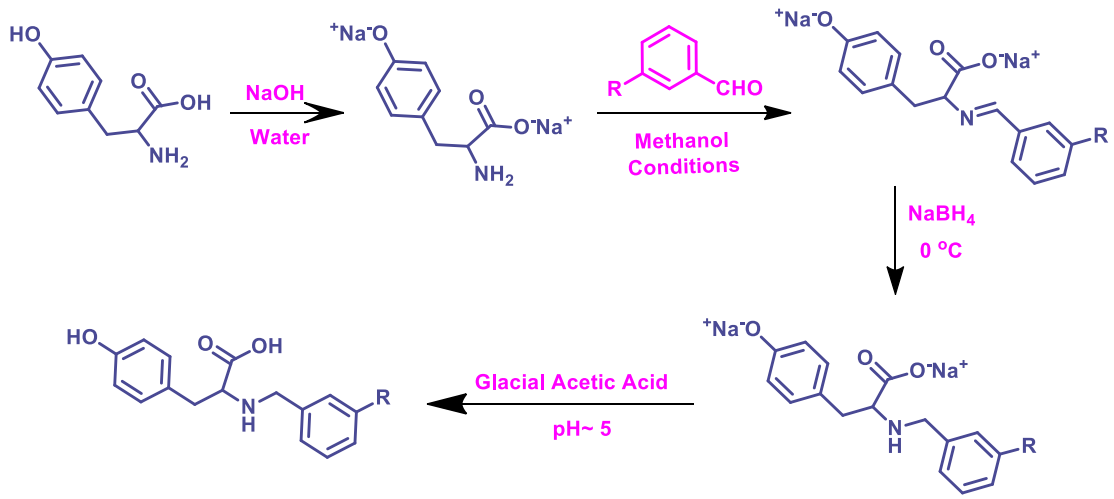

R	Condition	Ligand
NO_2	24 h, stir	L-H_2Tyr-3-nitro
Cl	5 h, reflux	L-H_2Tyr-3-chloro
OCH_3	6 h, reflux	L-H_2Tyr-3-methoxy

Scheme 1. General synthesis of ligands.

$$ZnSO_4{\cdot}7H_2O + 2\ \text{L-}H_2\text{Tyr-3-X} + 2\ NaOH \xrightarrow[\text{Stir, 24 h}]{\text{Water}} [Zn(\text{L-HTyr-3-X})_2(H_2O)] + Na_2SO_4 + 8\ H_2O$$

X = nitro (**1**); X = chloro (**3**); X = methoxy (**5**)

$$Cd(OAc)_2{\cdot}2H_2O + 2\ \text{L-}H_2\text{Tyr-3-X} + 2\ NaOH \xrightarrow[\text{Stir, 24 h}]{\text{Water}} [Cd(\text{L-HTyr-3-X})_2(H_2O)] + NaOAc + 3\ H_2O$$

X = nitro (**2**); X = chloro (**4**); X = methoxy (**6**)

Scheme 2. General synthesis of metal complexes **1**-**6**.

For L-H_2Tyr-3-chloro, the aromatic region has 8 H of four types in the aromatic region. 3 H at 7.2 ppm and 1 H at 7.0 ppm correspond to the phenyl ring containing the chloro group. Due to the presence of electron donating group (chloro) these are observed at less downfield. At 6.7 and 6.5 ppm, 2 H each are observed for the phenolic group of tyrosine. In the non-aromatic region, a total of five protons of four different types are observed. Two protons of the -CH_2 group of the phenyl moiety are split due to the presence of diastereomers (1 H at 3.4 ppm and 1 H at 3.6

ppm). The proton of the -CH group of chiral carbon centre is observed at 3.1 ppm and the two protons of the -CH_2 group attached with the phenolic group of tyrosine appear at 2.6 ppm.

For L-H_2Tyr-3-methoxy, the aromatic region has 8 H of three types in the aromatic region. 1 H at 7.1 ppm corresponds to the phenyl ring containing the methoxy group, at 6.7 ppm, 5 H are mixed together with 3 H from the phenyl ring containing the methoxy group and a 2 H from the phenolic group of tyrosine. Due to the presence of methoxy group on the phenyl ring that has a positive inductive effect and negative resonance effect, the protons are shifted upfield. At 6.4 ppm 2 H observed from the phenolic group of tyrosine. In the non-aromatic region, a total of eight protons of five different types are observed. 3 H corresponding to the methoxy group appear at 3.7 ppm. The two protons of the -CH_2 group of the phenyl moiety are split due to the presence of diastereomers (1 H at 3.4 ppm and 1 H at 3.6 ppm). The proton of the -CH group of chiral carbon centre is observed at 3.1 ppm and the two protons of the -CH_2 group attached with the phenolic group of tyrosine appear at 2.6 ppm.

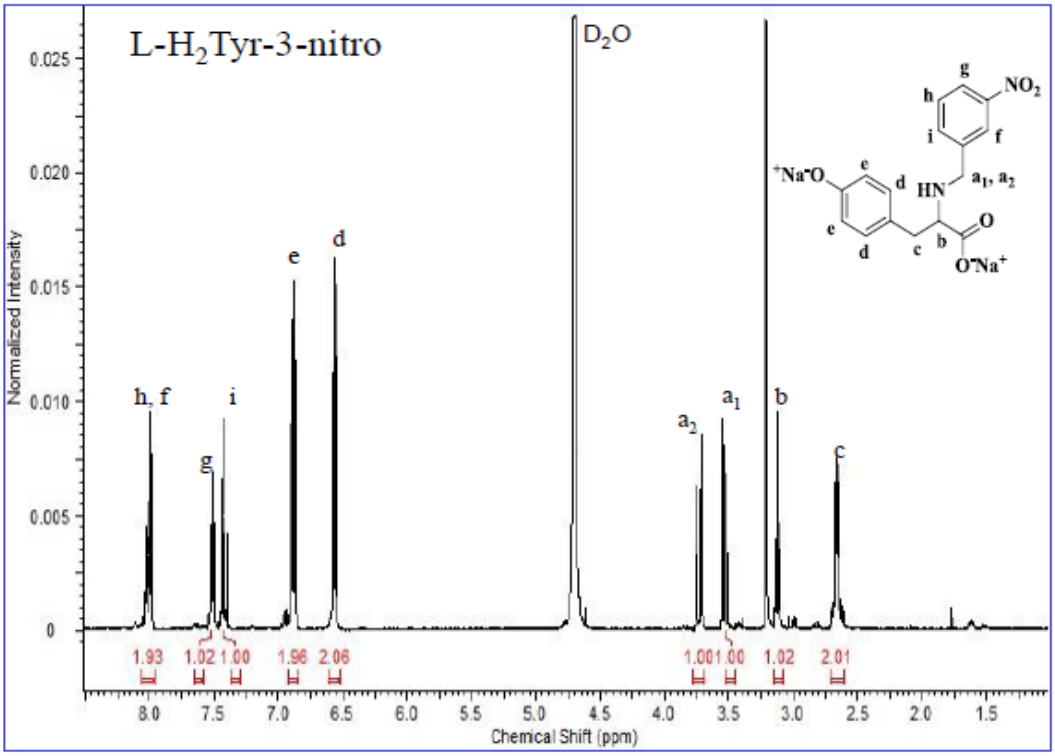

Figure 8. ^{1}H NMR spectrum of L-H_2Tyr-3-nitro.

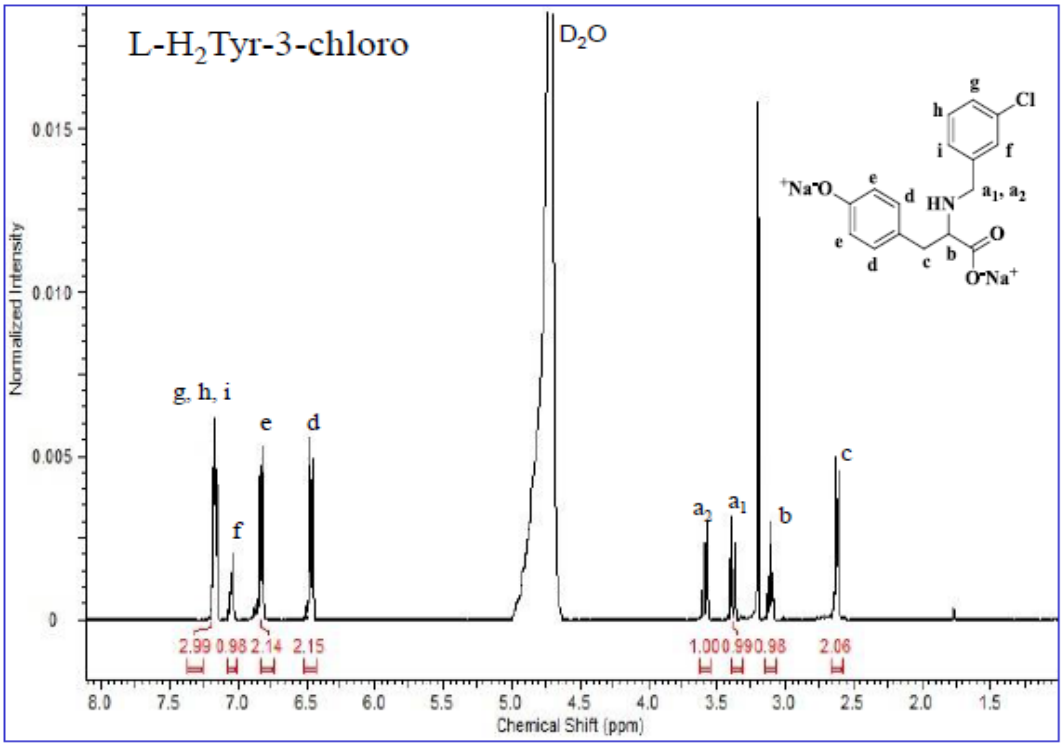

Figure 9. ^{1}H NMR spectrum of L-H_2Tyr-3-Chloro.

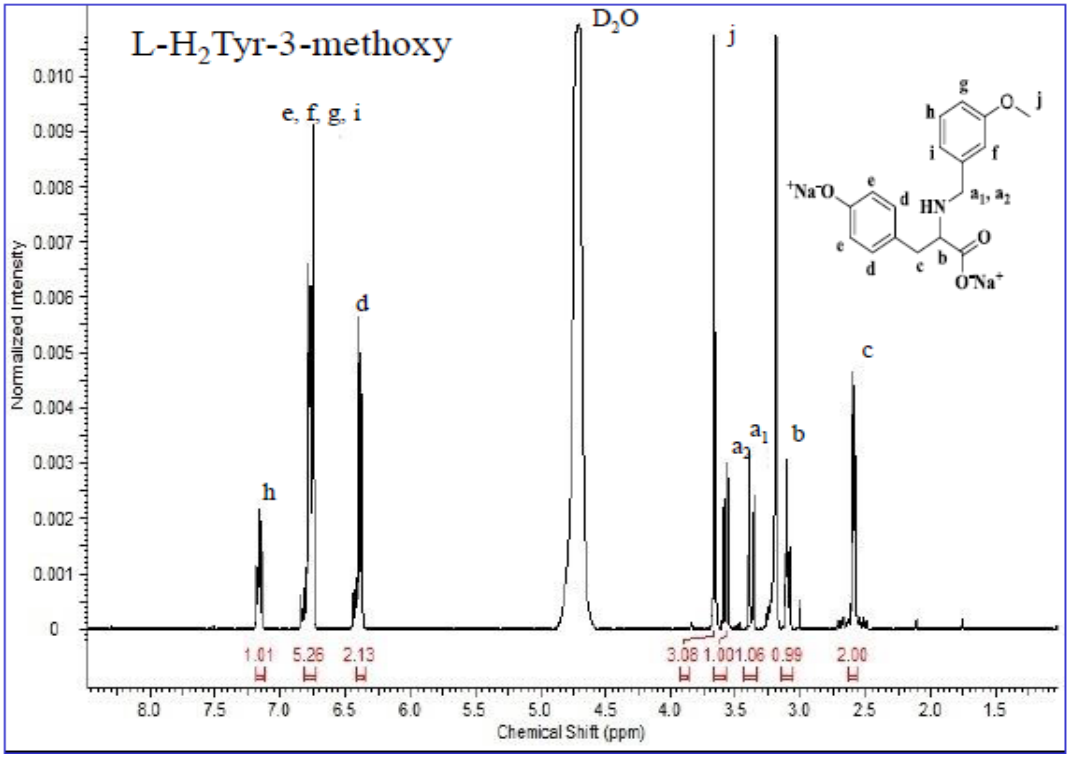

Figure 10. ^{1}H NMR spectrum of L-H_2Tyr-3-methoxy.

FTIR Spectroscopy

A broad peak at around 3400 cm^{-1}, corresponding to the O-H stretching frequency of water, is observed in the FTIR spectra of ligands as well as the metal complexes (Figures 11-19). The feature around 3200 cm^{-1} shows the presence of coordinated water molecules. In complex **1**, the peak at 3448 cm^{-1} is sharper than that for other complexes. The peak around 2930 cm^{-1} corresponds to the N-H stretch of the ligands.

The difference between the asymmetric and symmetric stretching frequencies of the carboxylate groups ($\Delta\nu$ value) in metal complexes is calculated to predict the binding mode of the carboxylate group (see Table 1 and Figures 11-19). As an example, the asymmetric and the symmetric stretching for the carboxylate in **1** that appear at 1586 cm^{-1} and 1347 cm^{-1}, respectively, provides the $\Delta\nu$ (cm^{-1}) = ν_{COO^-} asymm - ν_{COO^-} symm = 239 cm^{-1}. Based on the literature values for such systems,[14] in all cases the carboxylate group is found to coordinate to the metal center in a monodentate fashion. The N-O stretch at 1525 cm^{-1} is observed in case of L-HTyr-3-nitro and its metal complexes **1** and **2,** as shown in Figure 11 and Figures 14 and 15, respectively. In L-HTyr-3-chloro, C-Cl bond stretch is observed at 829 cm^{-1} (Figure 12).

Table 1. Comparison of the carboxylat**e** binding modes of **1**-**6**.

Metal complexes	ν_{COO^-} asymm (cm^{-1})	ν_{COO^-} symm (cm^{-1})	$\Delta\nu$ (cm^{-1})	Binding mode
[Zn(L-HTyr-3-nitro)$_2$(H_2O)]·4H_2O (**1**·4H_2O)	1598	1350	248	Monodentate
[Cd(L-HTyr-3-nitro)$_2$(H_2O)]·3H_2O (**2**·3H_2O)	1585	1352	233	Monodentate
[Zn(L-HTyr-3-chloro)$_2$(H_2O)]·2H_2O (**3**·2H_2O)	1599	1395	204	Monodentate
[Cd(L-HTyr-3-chloro)$_2$(H_2O)]·2H_2O (**4**·2H_2O)	1587	1396	191	Monodentate
[Zn(L-HTyr-3-methoxy)$_2$(H_2O)]·3H_2O (**5**·3H_2O)	1596	1397	199	Monodentate
[Cd(L-HTyr-3-methoxy)$_2$(H_2O)]·2H_2O (**6**·2H_2O)	1589	1387	202	Monodentate

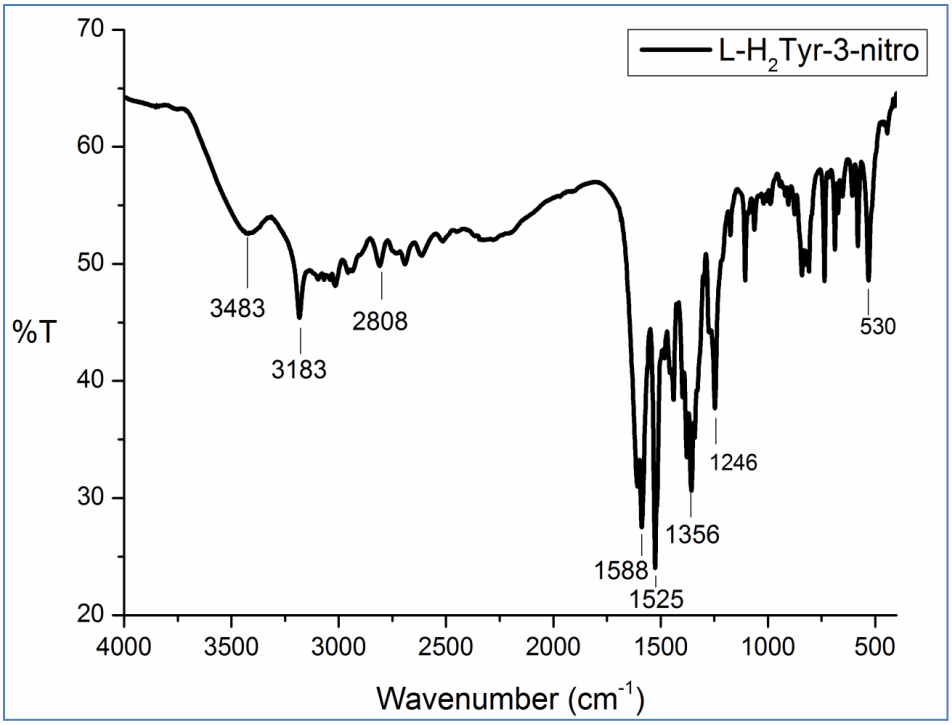

Figure 11. FTIR spectrum of L-H_2Tyr-3-nitro.

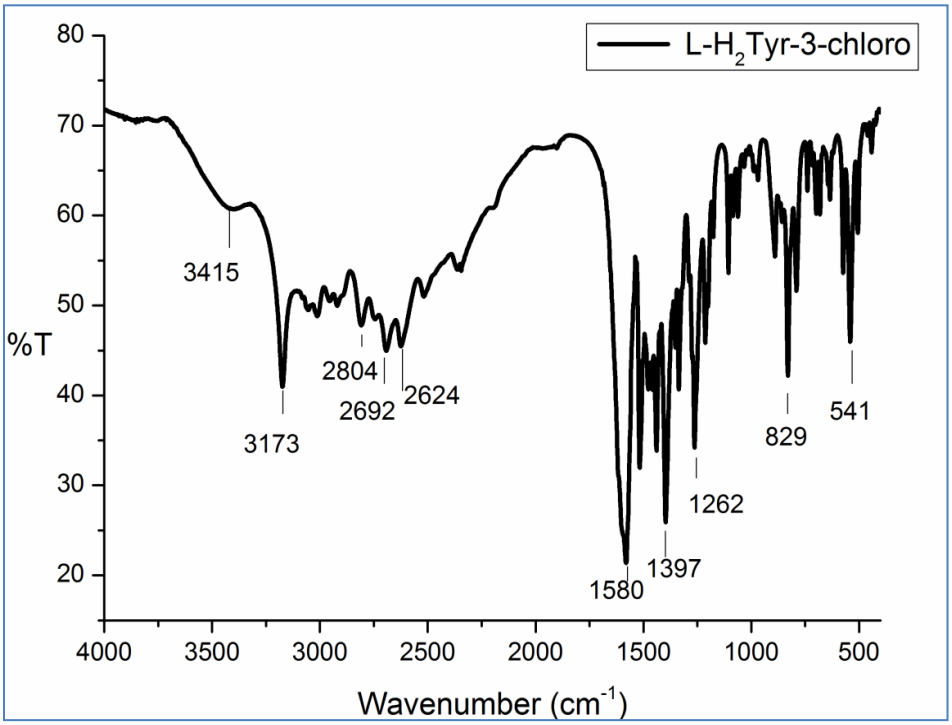

Figure 12. FTIR spectrum of L-H_2Tyr-3-chloro.

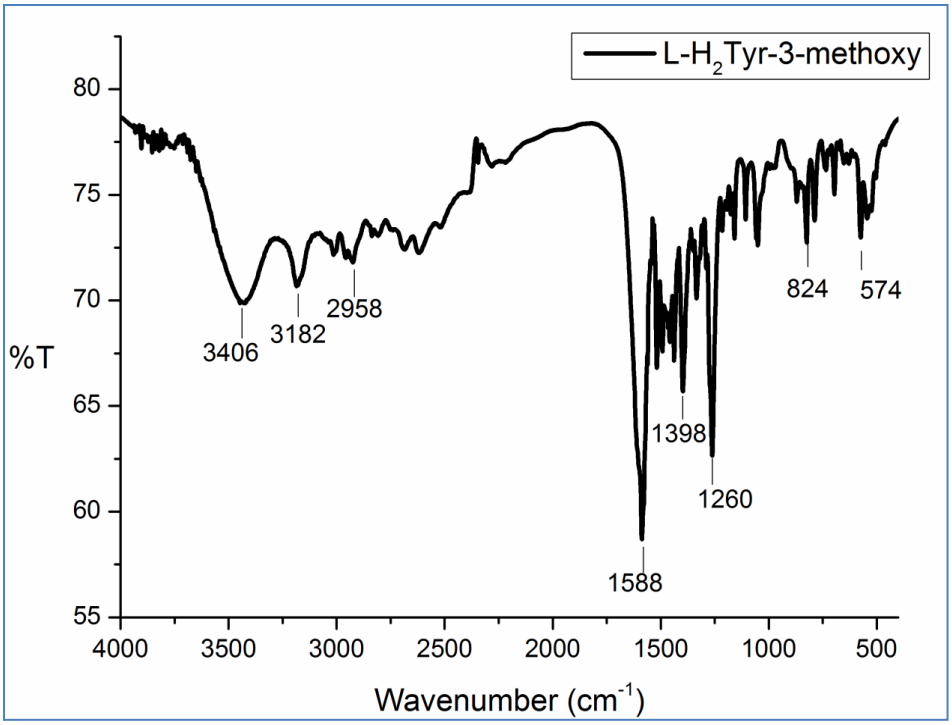

Figure 13. FTIR spectrum of L-H_2Tyr-3-methoxy.

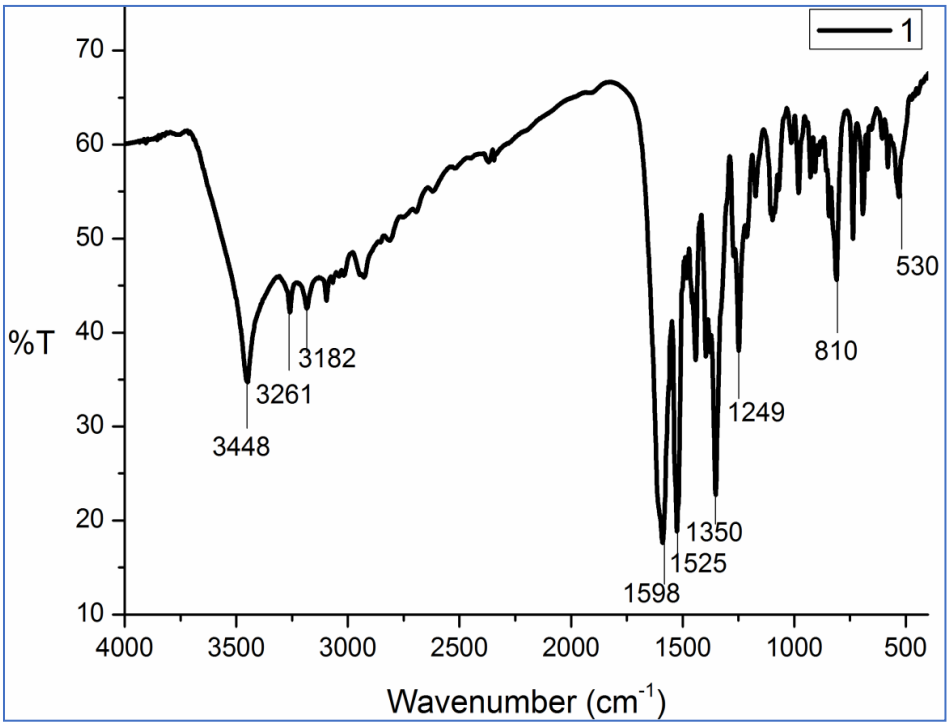

Figure 14. FTIR spectrum of **1**.

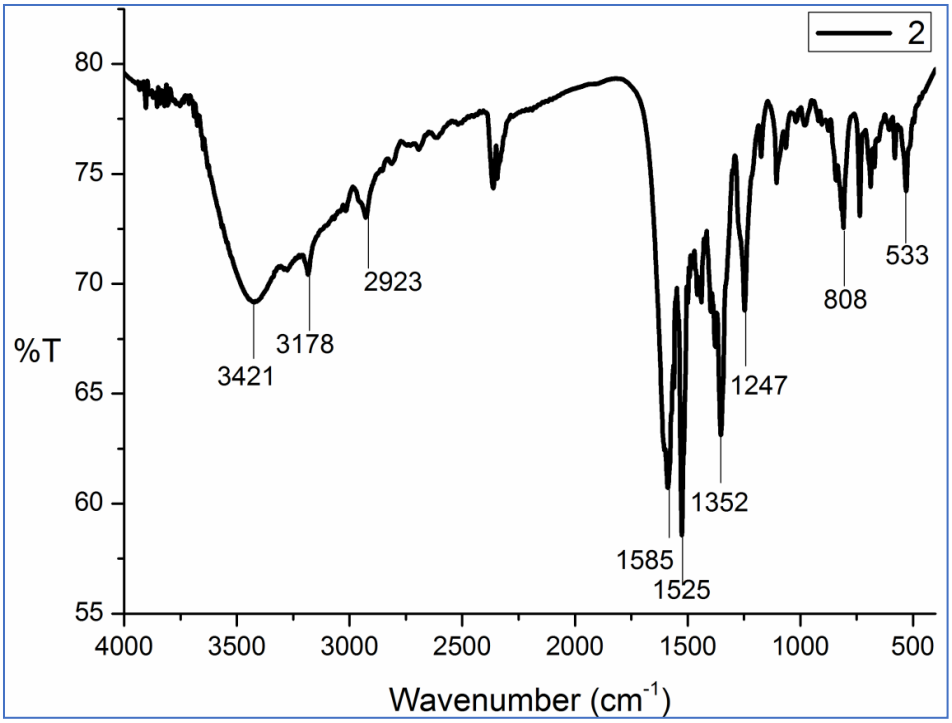

Figure 15. FTIR spectrum of **2**.

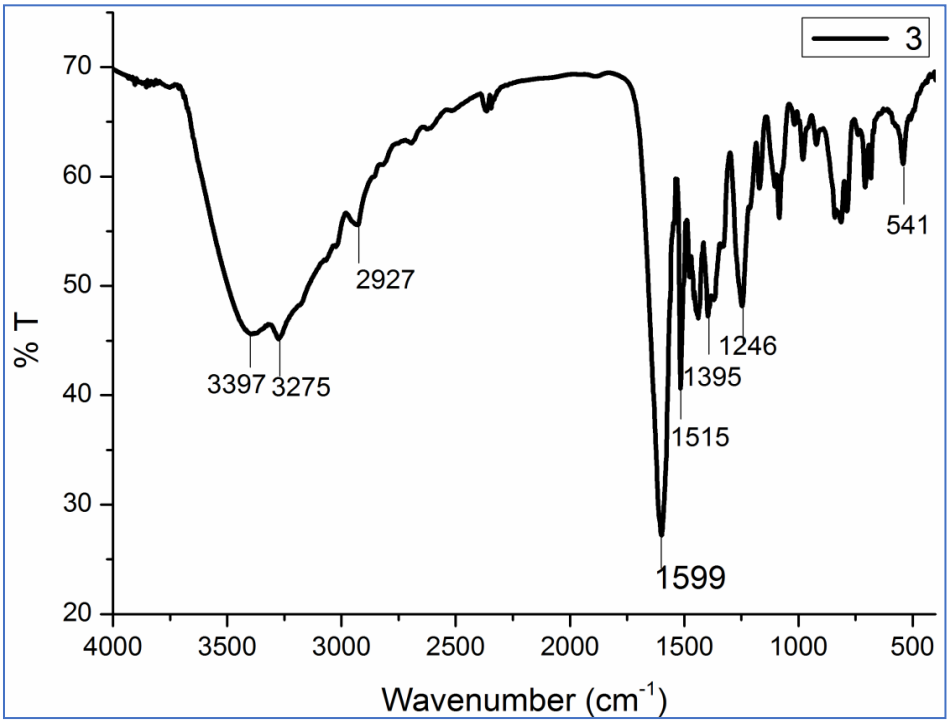

Figure 16. FTIR spectrum of **3**.

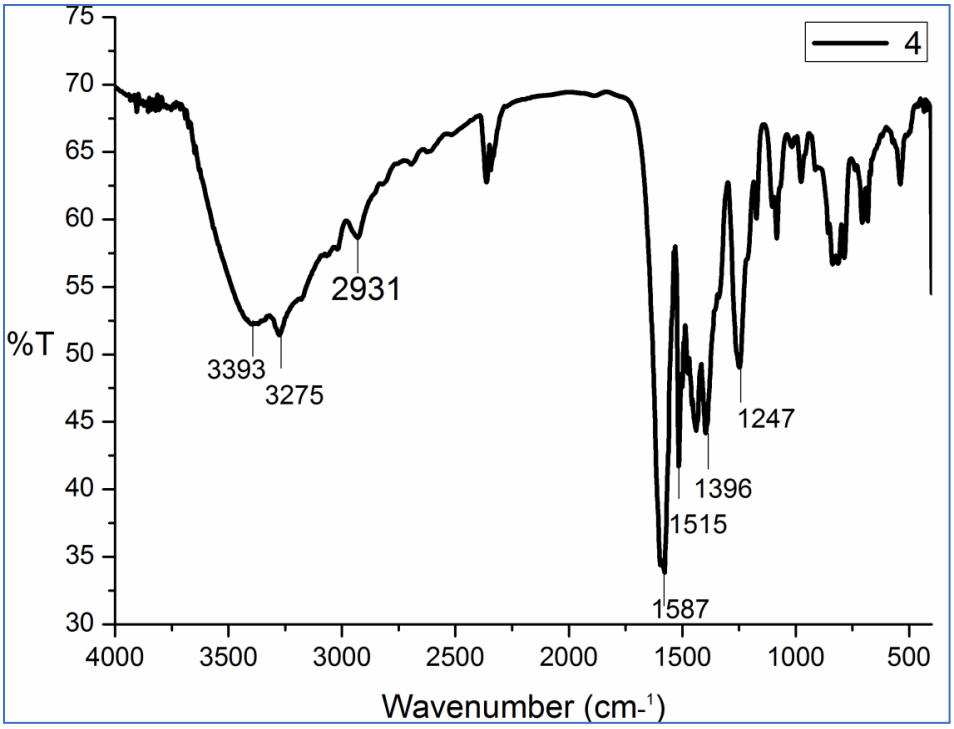

Figure 17. FTIR spectrum of **4**.

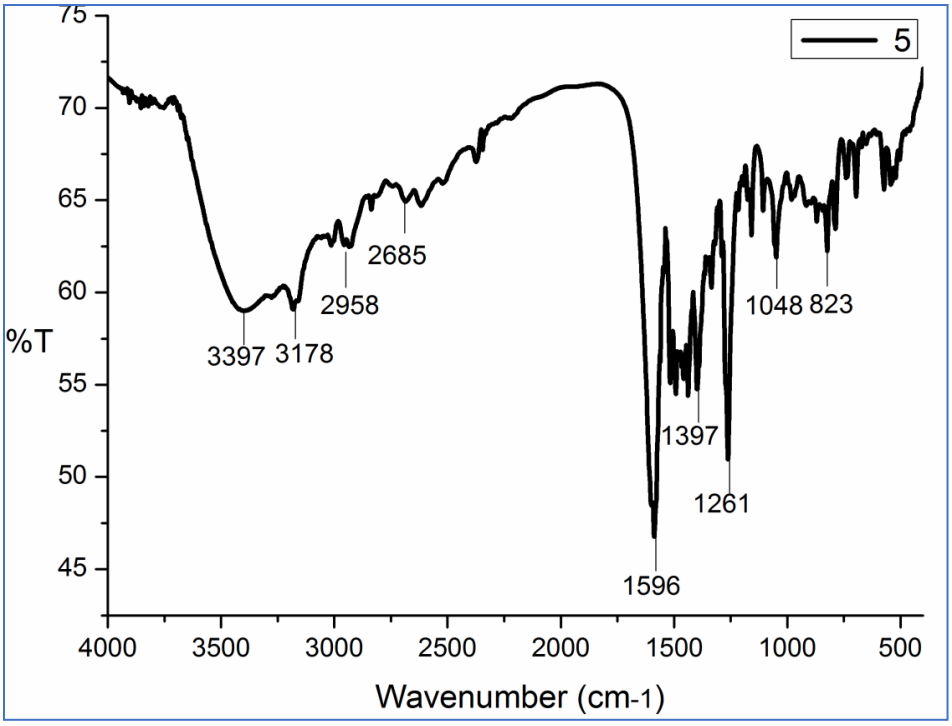

Figure 18. FTIR spectrum of **5**.

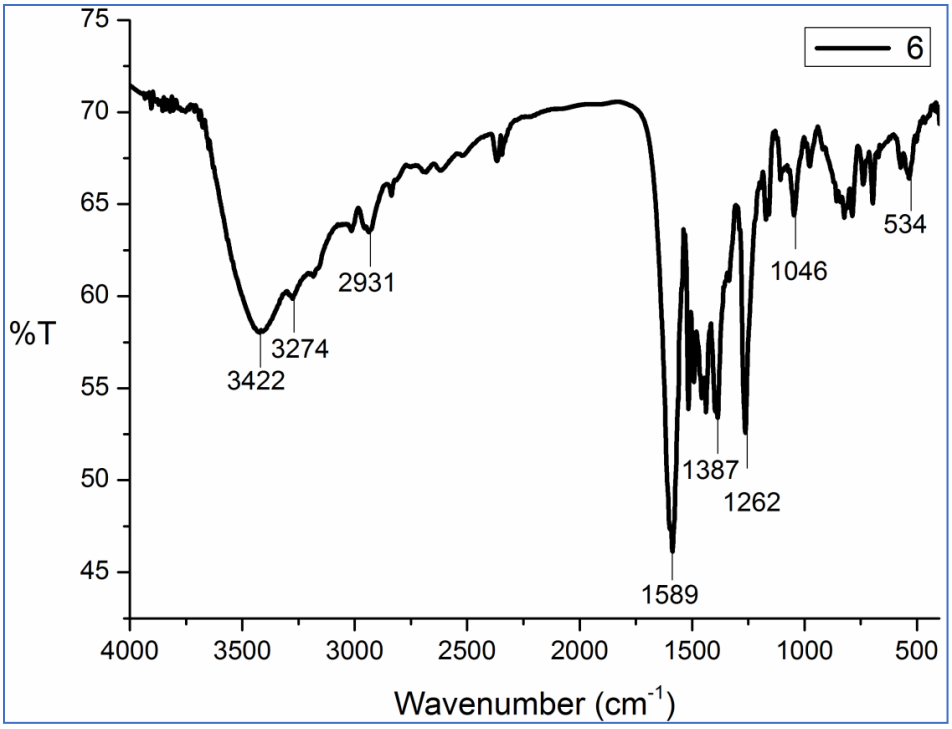

Figure 19. FTIR spectrum of **6**.

Powder X-ray Diffractometry (PXRD)

Powder X-ray diffraction was used to analyze the crystalline nature of ligands as well as their metal complexes. All the ligands (L-H_2Tyr-3-nitro, L-H_2Tyr-3-chloro and L-H_2Tyr-3-methoxy) showed crystalline nature (Figure 20) whereas in case of metal complexes only **1** (Figure 21) and **2** (Figure 22) showed crystallinity. The rest of the metal complexes were found to be amorphous in nature.

UV-Vis Spectroscopy

Most of the organic ligands show absorbance in the UV region that can be attributed to the π–π* transitions. Tyrosine shows two absorbance maxima at 270 nm and 220 nm. The three new ligands based on tyrosine reported in this work also show the π–π* transitions at 270 nm and 220 nm. In case of L-H_2Tyr-3-nitro, due to the electron withdrawing nitro group on the phenyl ring, the energy gap between LUMO and HOMO decreases, leading to an increased transition probability and higher absorbance. In case of the chloro and the methoxy derivatives, these electron donating groups lead to an increase in the energy gap between LUMO and HOMO, and

thus show lower absorbance values. The UV-Vis absorbance spectra of the three ligands are shown in Figure 23.

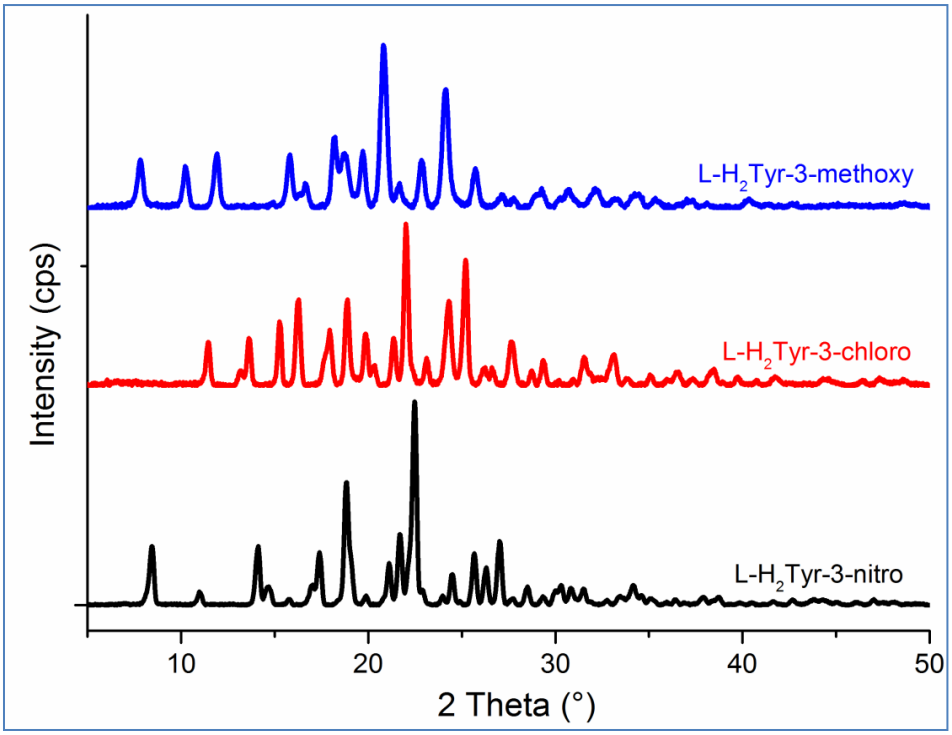

Figure 20. A comparison of PXRD patterns of the ligands.

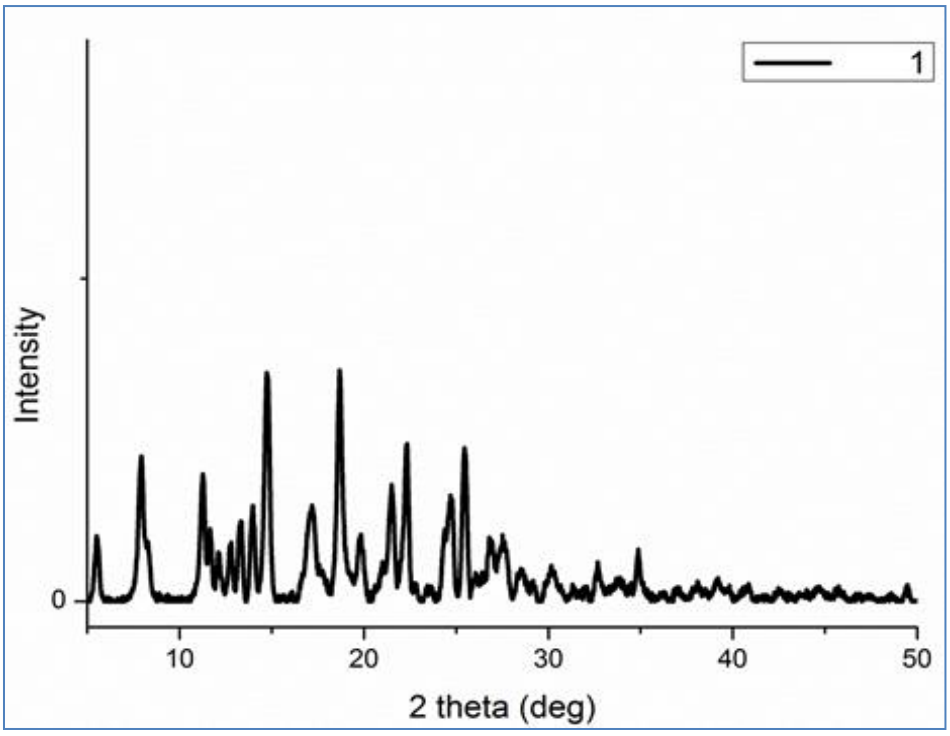

Figure 21. PXRD pattern of **1**.

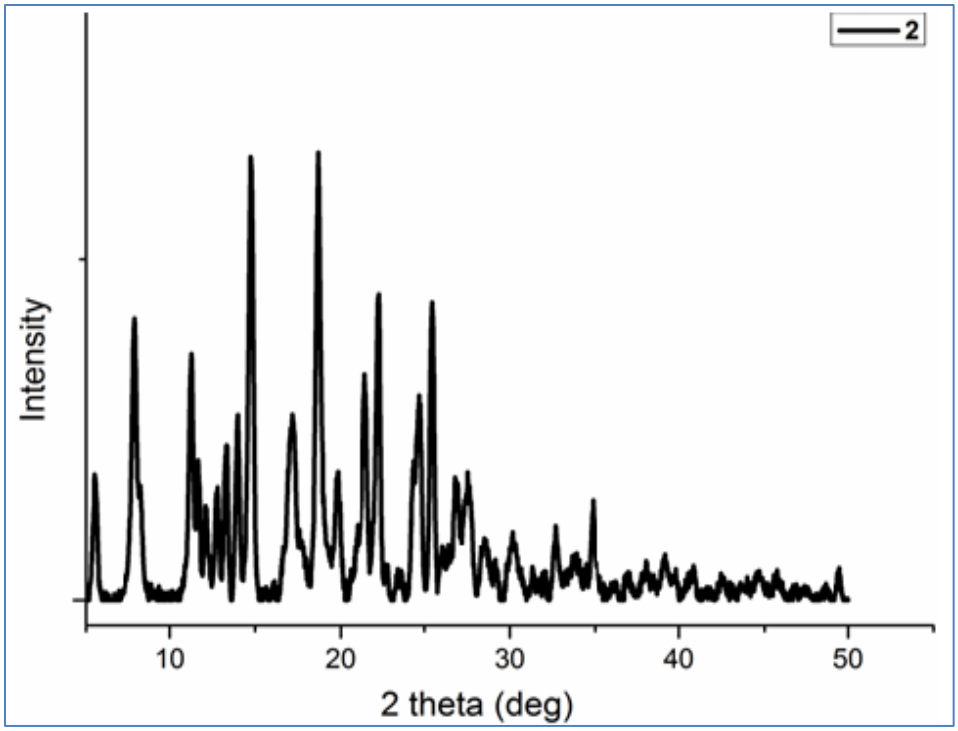

Figure 22. PXRD pattern of **2**.

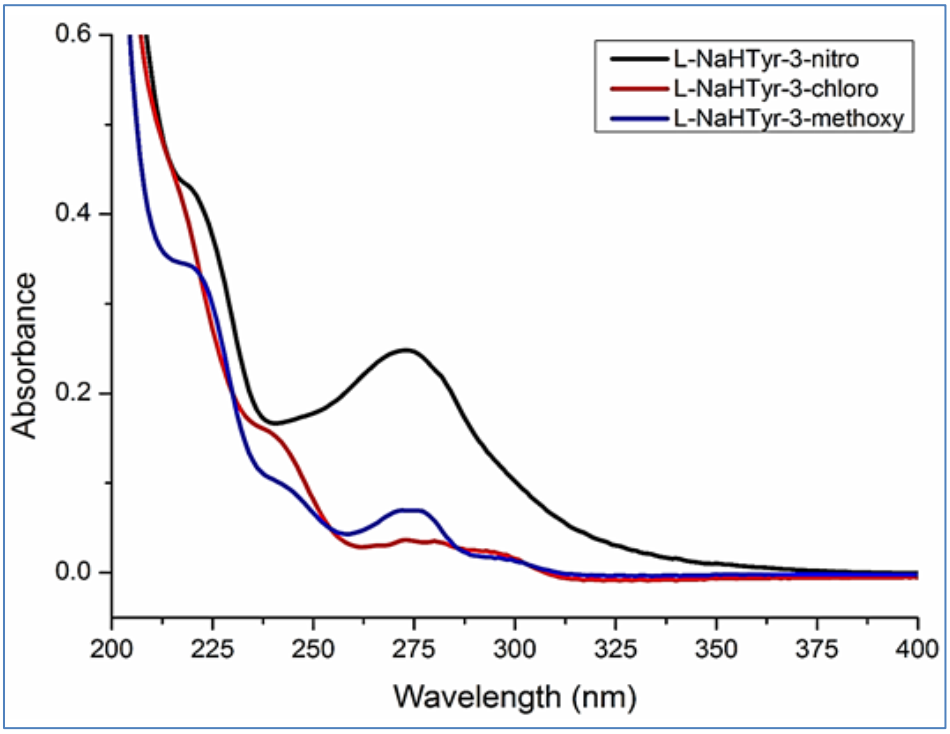

Figure 23. UV-Vis spectra of L-NaHTyr-3-nitro, L-NaHTyr-3-chloro and L-NaHTyr-3-methoxy (in water).

Fluorescence Spectroscopy

Based on the fluorescence property of the ligands (L-H_2Tyr-3-nitro, L-H_2Tyr-3-chloro and L-H_2Tyr-3-methoxy), shown in Figures 24-26, respectively, these were examined for their anion sensing ability in two different solvents.

Anion sensing by the ligands (in DMSO)

The ligand L-H_2Tyr-3-nitro showed the best fluorescence enhancement among the ligands, and the least enhancement was shown by L-H_2Tyr-3-chloro. This can be attributed to the anion–π interactions. In case of L-H_2Tyr-3-nitro, the nitro group being a good electron withdrawing group pulls the electron cloud and creates a positive charge on the ring. The anionic analytes thus can interact with the ring leading to fluorescence enhancement. In case of electron donating groups attached to the ring, such as chlorine, -I effect is induced. For L-H_2Tyr-3-methoxy, both strong –M and +I effects are in place so it has better anion–π interaction than L-H_2Tyr-3-chloro. Thus, the ligand L-H_2Tyr-3-nitro shows best interaction with the fluoride ion, followed by L-H_2Tyr-3-methoxy and least with L-H_2Tyr-3-chloro.

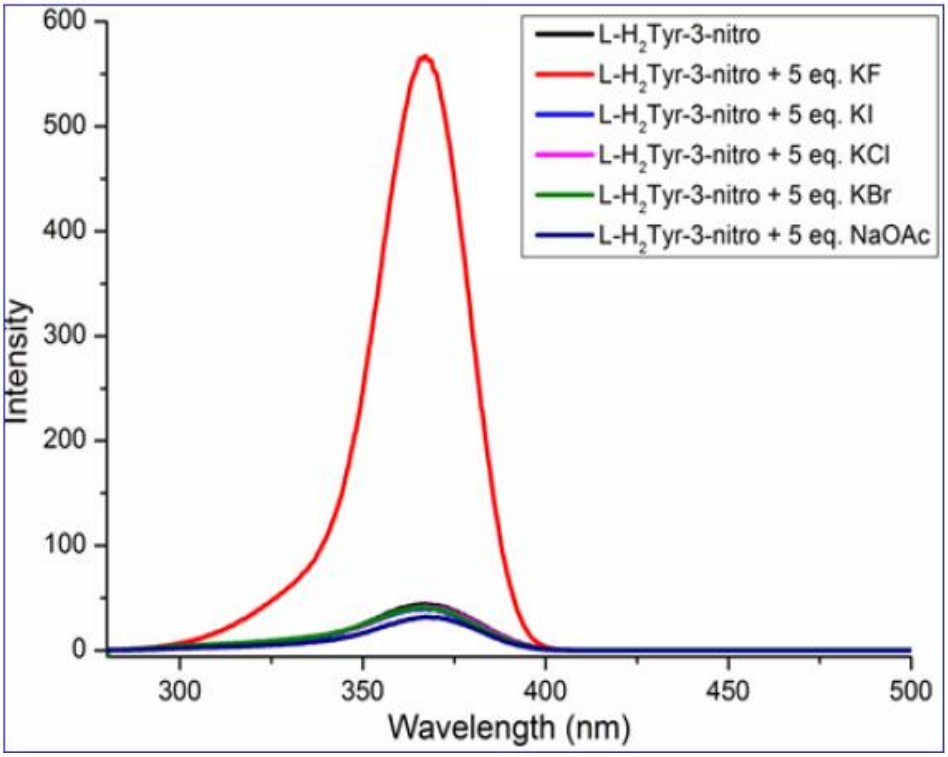

Figure 24. Fluorescence spectrum and anion sensing ability of L-H_2Tyr-3-nitro (λ_{exc} = 220 nm).

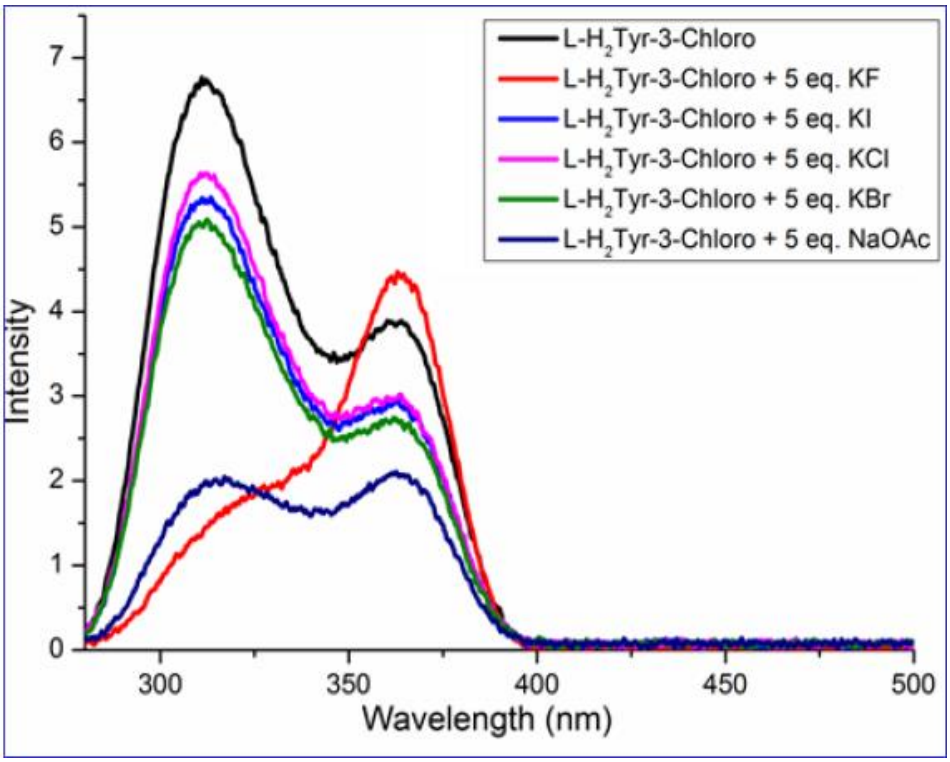

Figure 25. Fluorescence spectrum and anion sensing ability of L-H_2Tyr-3-chloro (λ_{exc} = 220 nm).

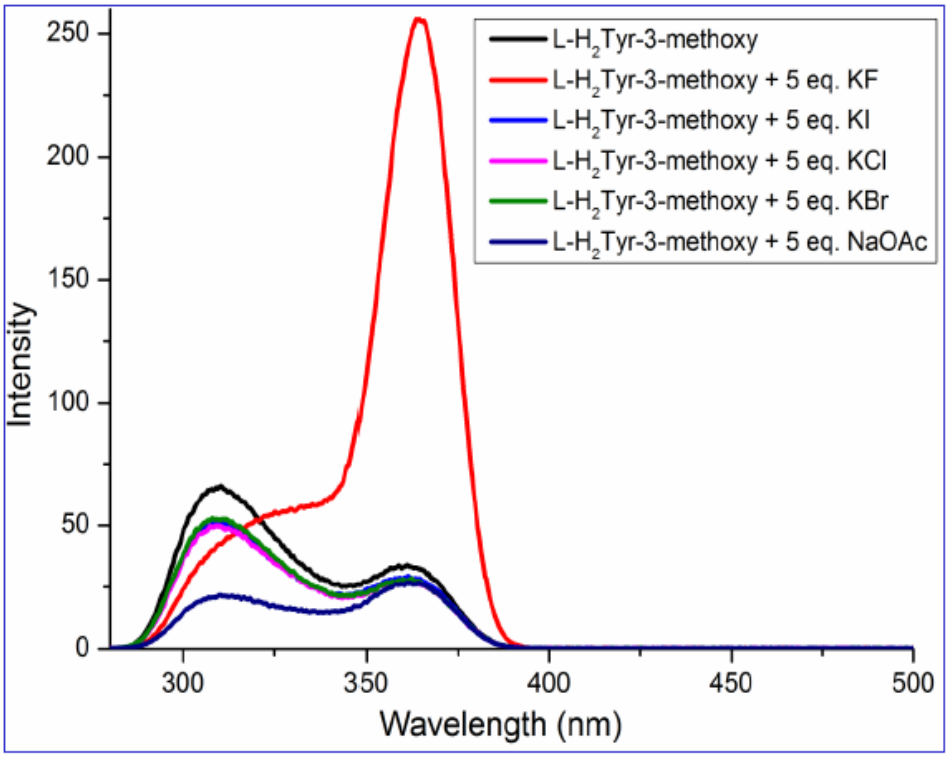

Figure 26. Fluorescence spectrum and anion sensing ability of L-H_2Tyr-3-methoxy (λ_{exc} = 220 nm).

In order to show the optimum equivalent amounts of different analytes required for the maximum fluorescence change by the ligands, the 3D plots in Figures 27-29, respectively, are

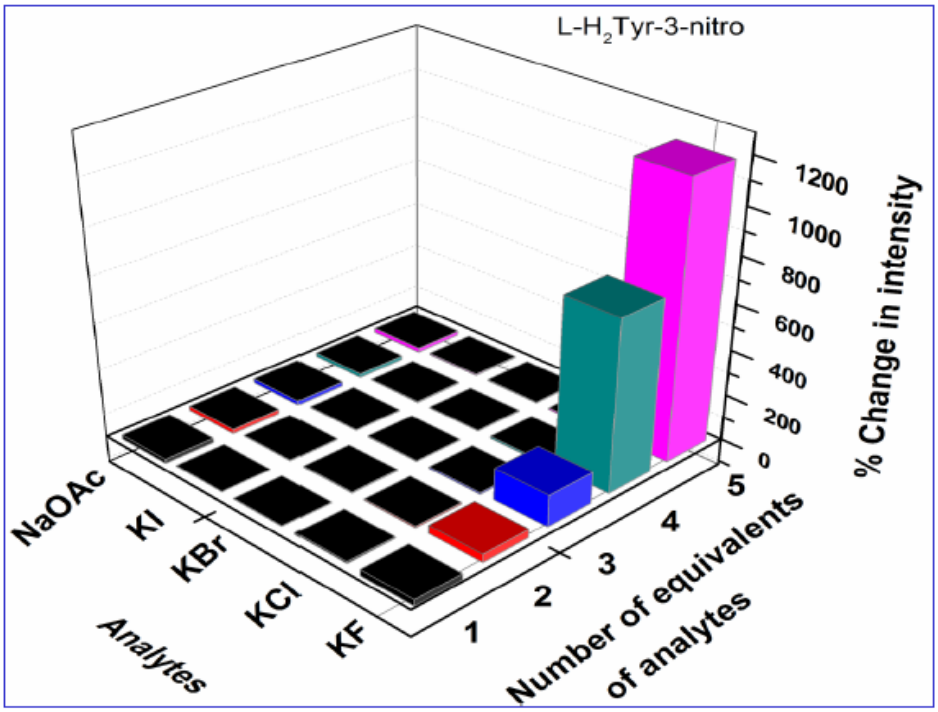

Figure 27. Representation of 3D plot of L-H_2Tyr-3-nitro (λ_{exc} = 220 nm , λ_{em} = 364 nm).

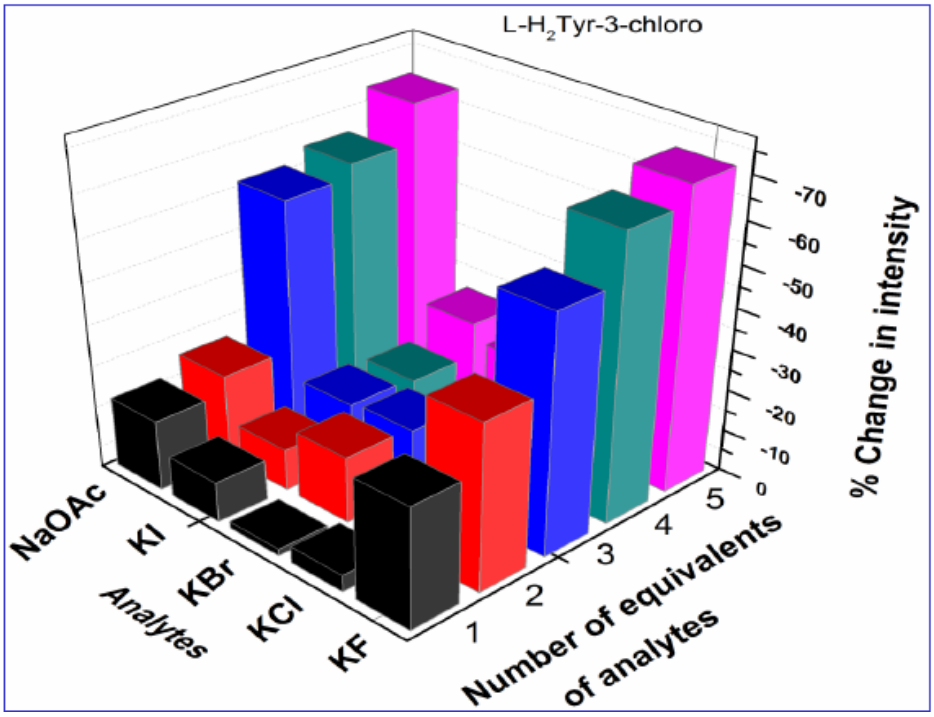

Figure 28. Representation of 3D plot of L-HTyr-3-chloro (λ_{exc} = 220 nm , λ_{em} = 364 nm).

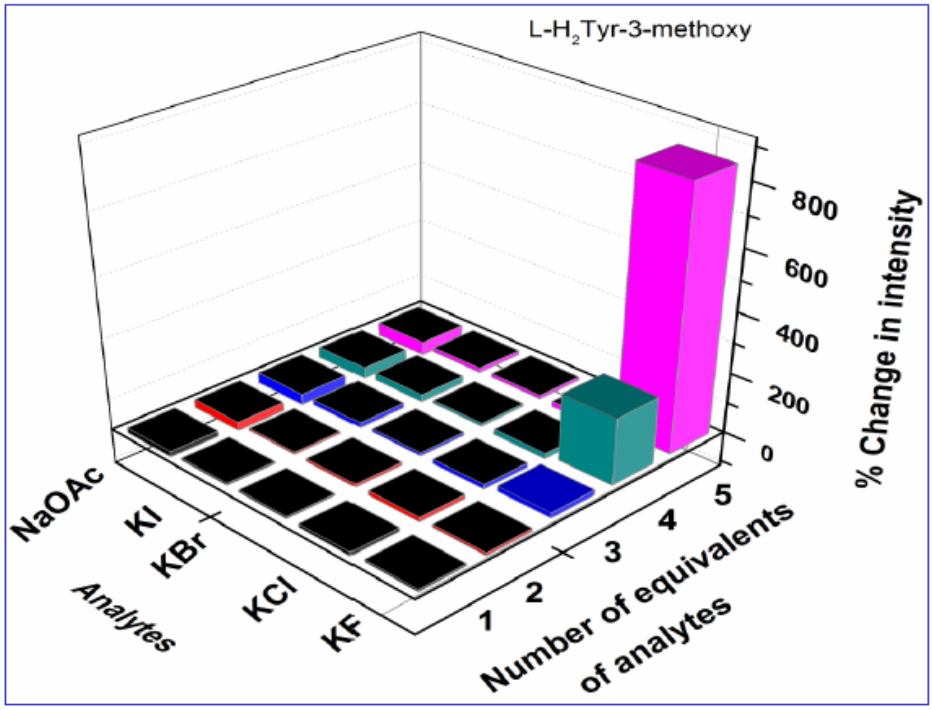

Figure 29. Representation of 3D plot of L-HTyr-3-methoxy (λ_{exc} = 220 nm , λ_{em} = 364 nm).

very helpful. As evident from these figures, with consecutive addition of KF a great increase in the fluorescence intensity is seen. On addition of 1 equivalent of KF, 15 % increase in the intensity is observed while addition of 5 eq of KF increased the intensity to 1200 %. Hence, L-H_2Tyr-3-nitro shows the best fluoride sensing ability compared to L-H_2Tyr-3-chloro and L-H_2Tyr-3-methoxy. On analyzing further, it is clear that the sensing of F^- over other anions is very selective for L-H_2Tyr-3-nitro and L-H_2Tyr-3-methoxy while that for L-H_2Tyr-3-chloro is equally good for F^- and OAc^-.

Anion sensing by the ligands (in methanol)

With methanol as the solvent, these ligands showed selective sensing for iodide ions (Figures 30-32). This shows that the solvent also plays a role in the behavior of the ligands towards sensing of the analytes. In this case, the ligand L-H_2Tyr-3-nitro also shows the best anion–π interaction, the reason being the same as described for DMSO, while the ligand L-H_2Tyr-3-chloro showed the least sensing and the ligand L-H_2Tyr-3-methoxy showed intermediate between these two. The sensing ability for iodide was further examined with iodide concentration up to 5 eq. and the resulting quenching with all the ligands is shown in Figures 30-32.

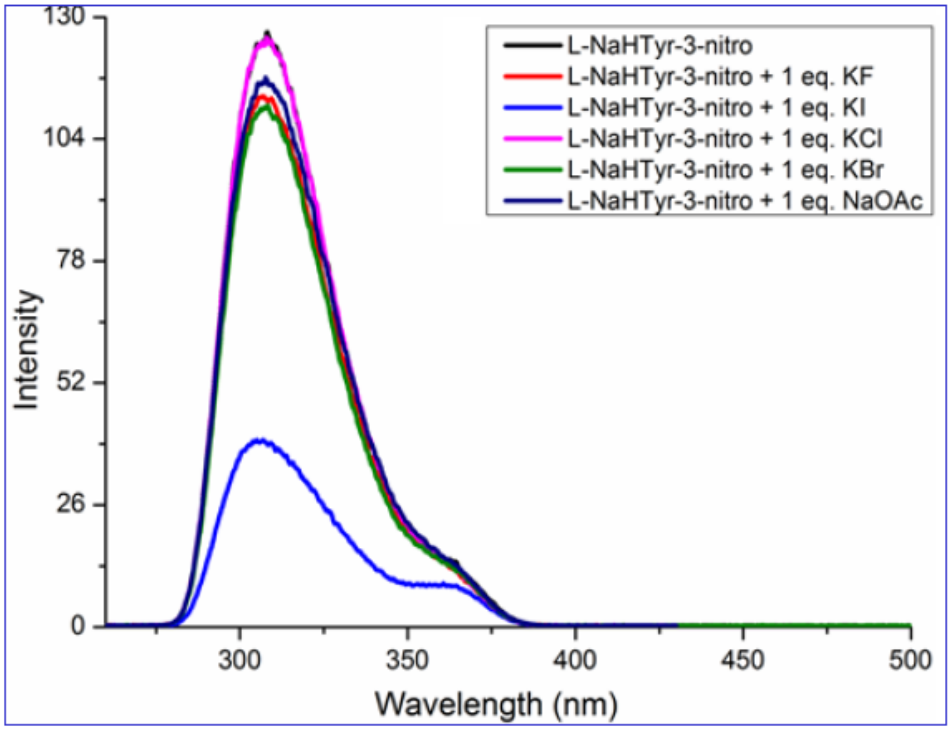

Figure 30. Fluorescence spectrum and anion sensing ability of L-NaHTyr-3-nitro in methanol (λ_{exc} = 220 nm).

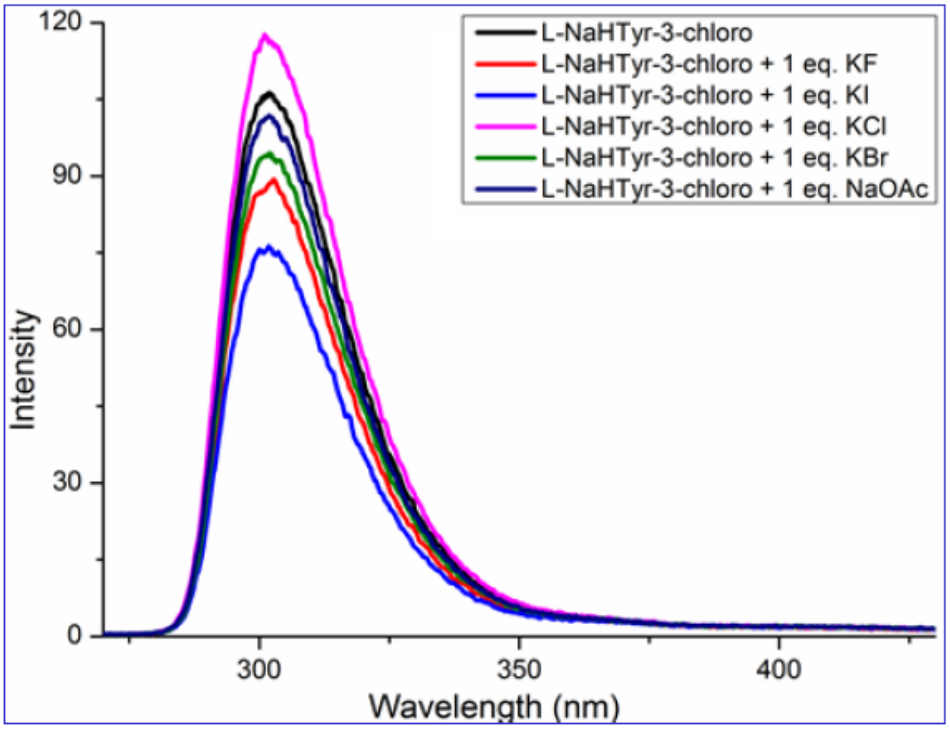

Figure 31. Fluorescence spectrum and anion sensing ability of L-NaHTyr-3-chloro in methanol (λ_{exc} = 220 nm).

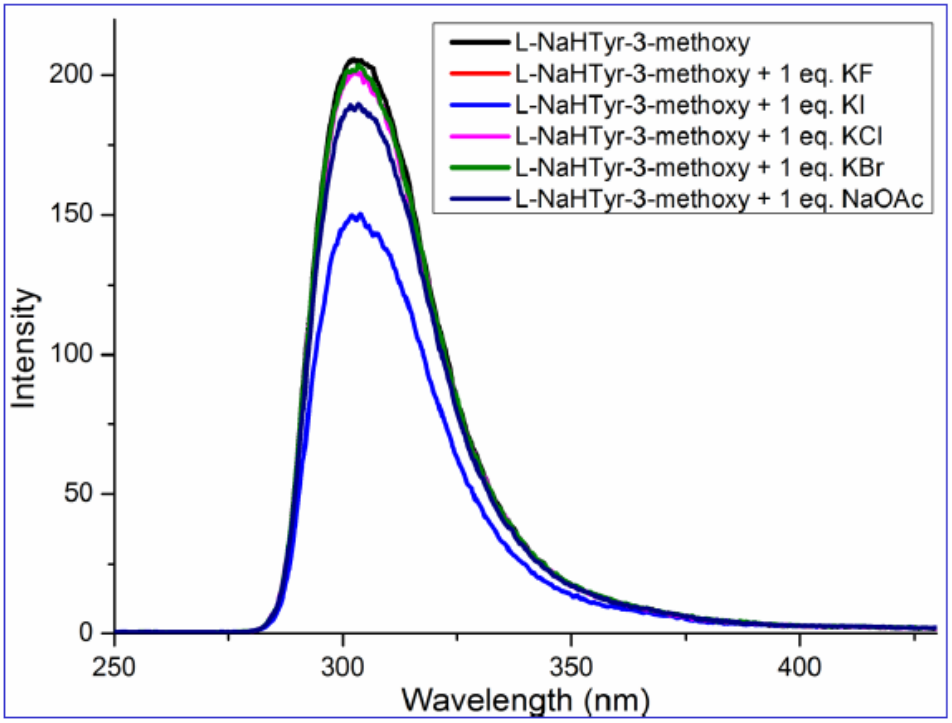

Figure 32. Fluorescence spectrum and anion sensing ability of L-NaHTyr-3-methoxy in methanol (λ_{exc} = 220 nm).

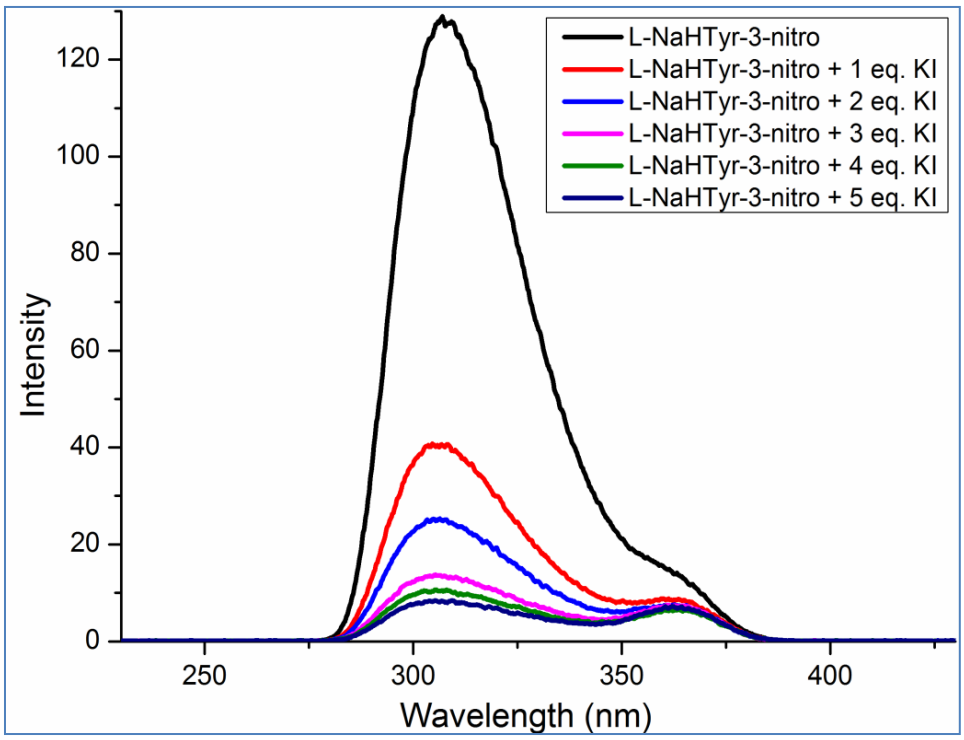

Figure 33. Fluorescence spectra for the sequential addition of KI to L-NaHTyr-3-nitro (λ_{exc} = 220 nm).

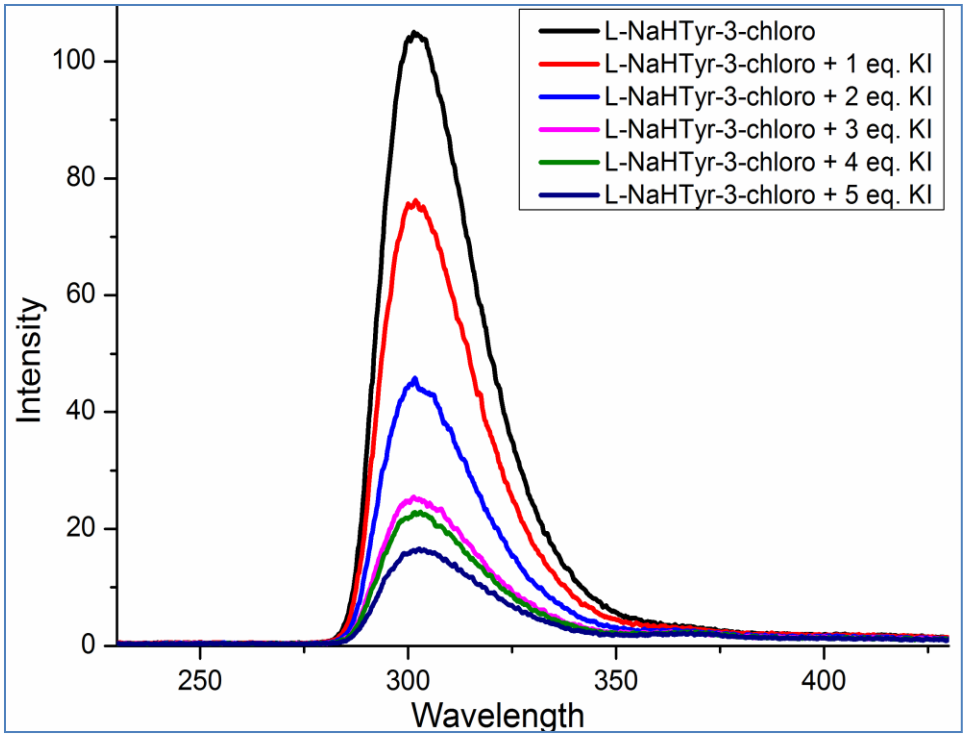

Figure 34. Fluorescence spectra for the sequential addition of KI to L-NaHTyr-3-chloro (λ_{exc} = 220 nm).

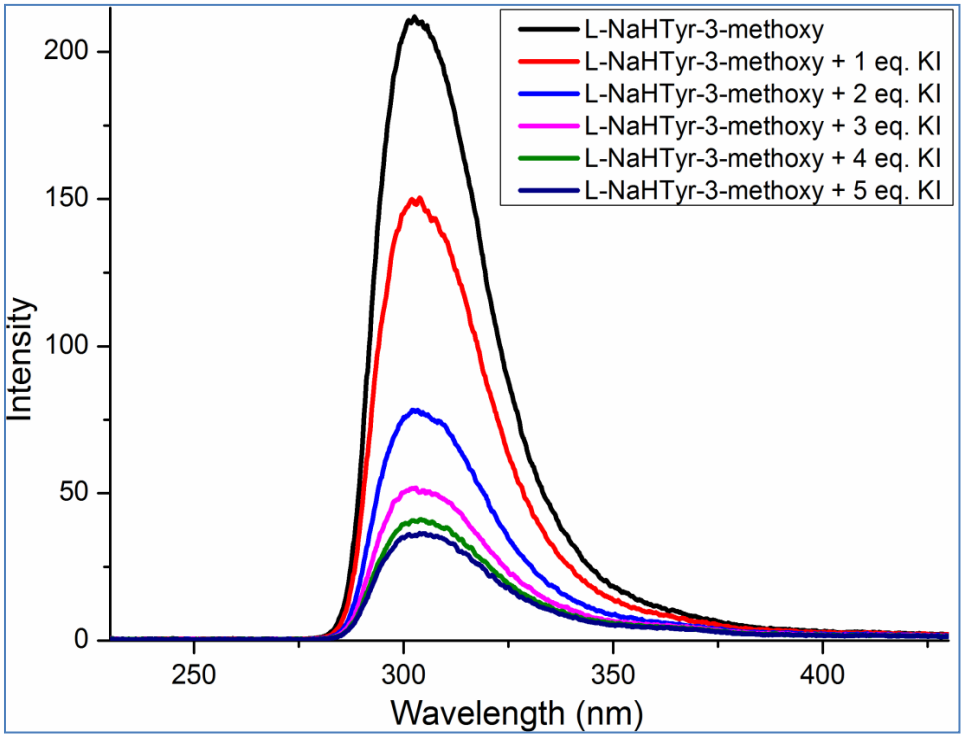

Figure 35. Fluorescence spectra for the sequential addition of KI to L-NaHTyr-3-methoxy (λ_{exc} = 220 nm).

Anion sensing by the metal complexes in DMSO

Anion sensing of the ligands are compared against their Zn(II) and Cd(II) complexes. In the literature it has been reported that the binding of metal ions Zn(II) and Cd(II) increases their fluorescence intensity. This can be attributed to the fact that these metals reduce the non-radiative pathways which enhance the fluorescence property. The metal complexes **1** and **3** did not show selective interaction for the analytes (see Figures 36 and 38, respectively), whereas the complexes **2**, **4**, **5** and **6** showed interaction between the metal complex and analyte (Figures 37 and 39-41, respectively). Furthermore, for a given ligand the Cd(II) complex was found to be better than the Zn(II) complex.

In order to understand the effect of different equivalents of analytes on the % of fluorescence enhancement of the metal complexes, 3D plots are generated for **2**, **4**, **5** and **6** (see Figures 42-45). In Figure 42, complex **2** shows much superior interaction of KF over the others and there is a drastic change in the enhancement between three and four eqv of KF. A similar trend is observed for **5** and **6** between four and five eqv of KF. On the other hand, a gradual change is observed for **4**. As expected, the best enhancement is observed for **2** containing the ligand L-HTyr-3-nitro.

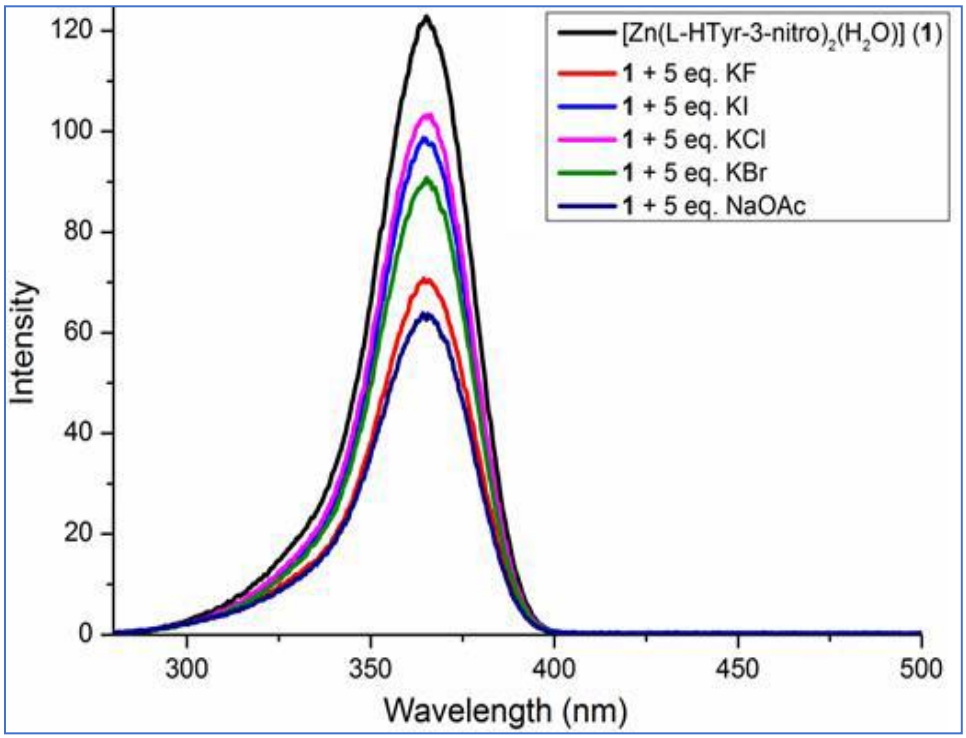

Figure 36. Fluorescence spectrum and anion sensing ability of **1** (λ_{exc} = 220 nm).

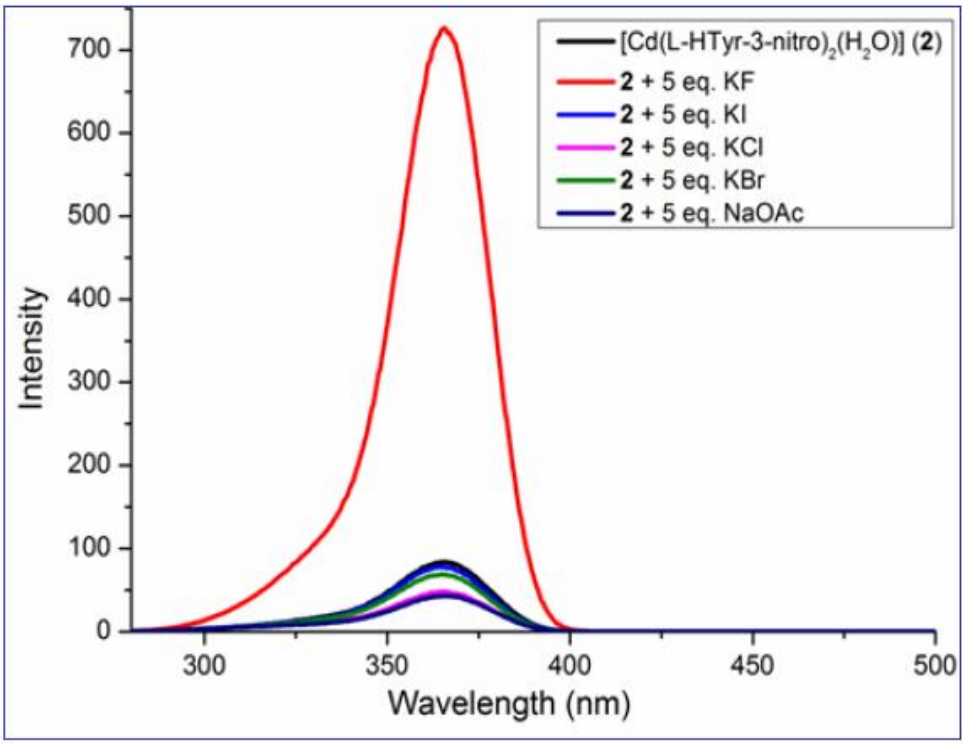

Figure 37. Fluorescence spectrum and anion sensing ability of **2** (λ_{exc} = 220 nm).

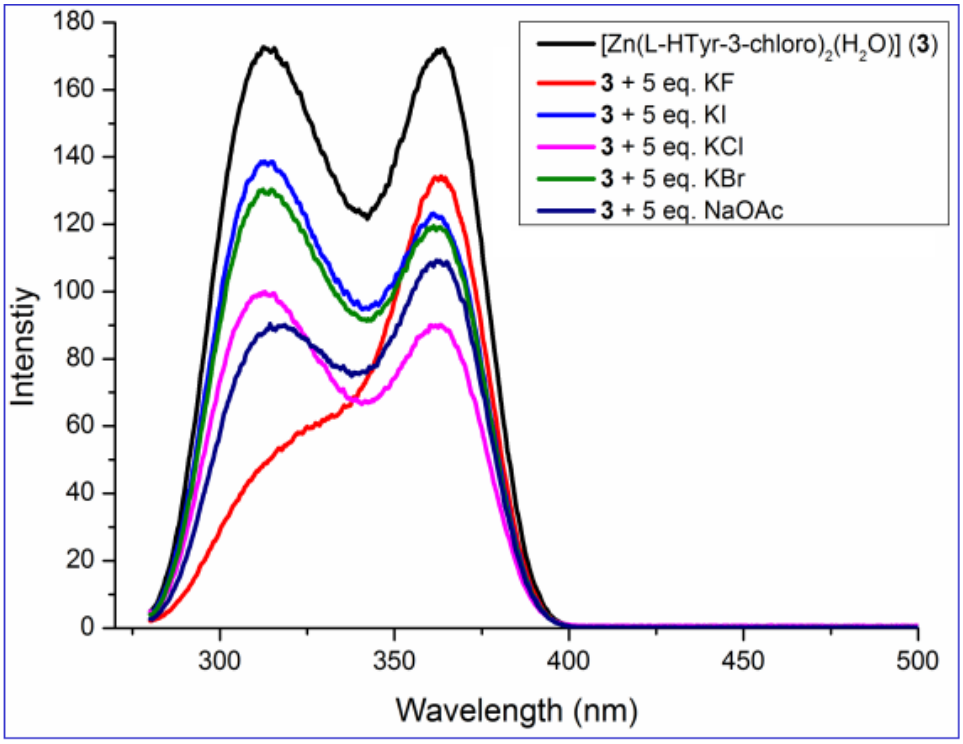

Figure 38. Fluorescence spectrum and anion sensing ability of **3** (λ_{exc} = 220 nm).

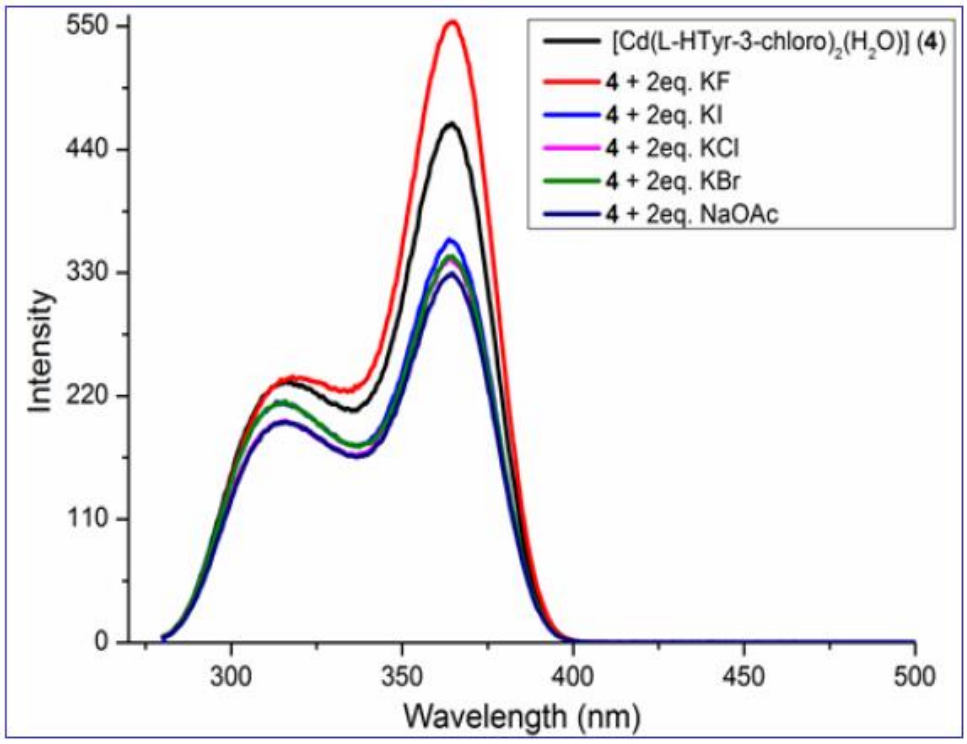

Figure 39. Fluorescence spectrum and anion sensing ability of **4** (λ_{exc} = 220 nm).

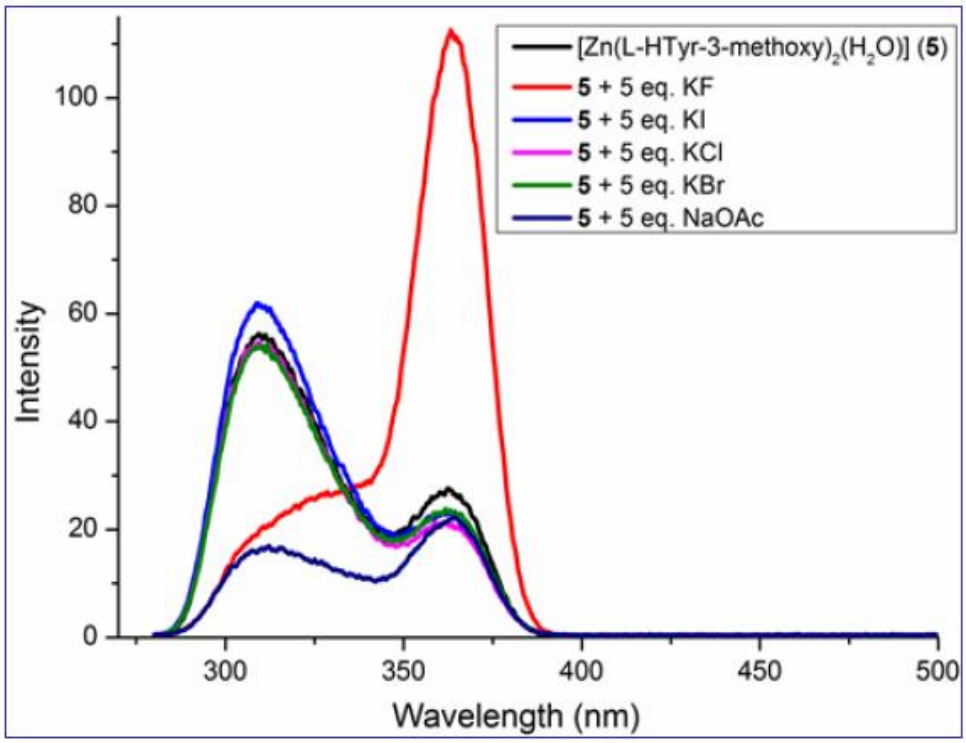

Figure 40. Fluorescence spectrum and anion sensing ability of **5** (λ_{exc} = 220 nm).

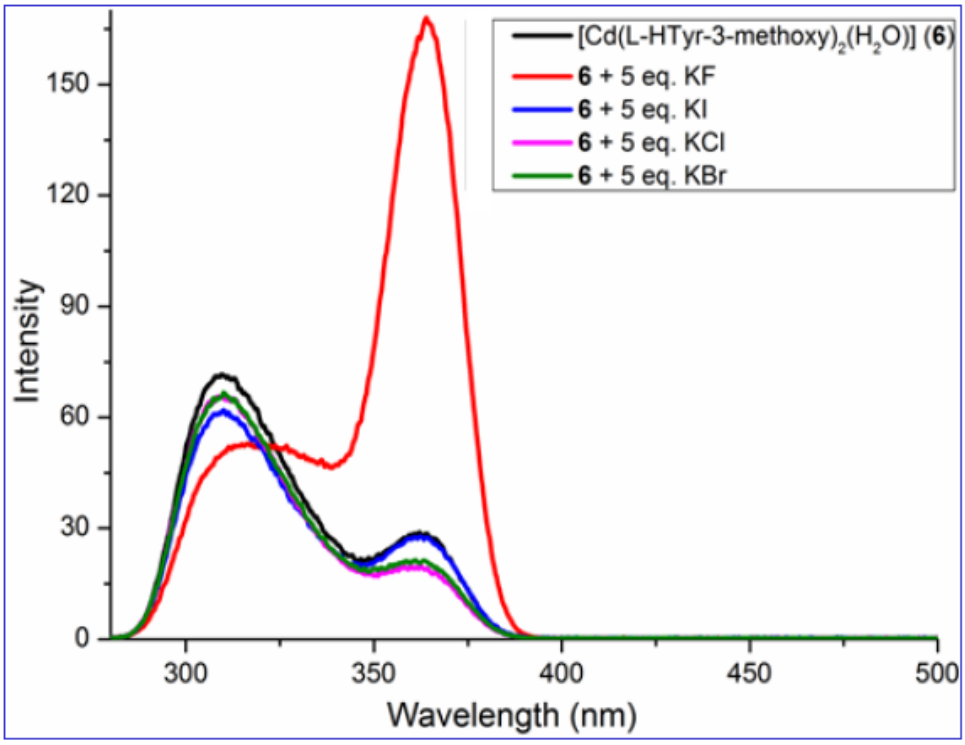

Figure 41. Fluorescence spectrum and anion sensing ability of **6** (λ_{exc} = 220 nm).

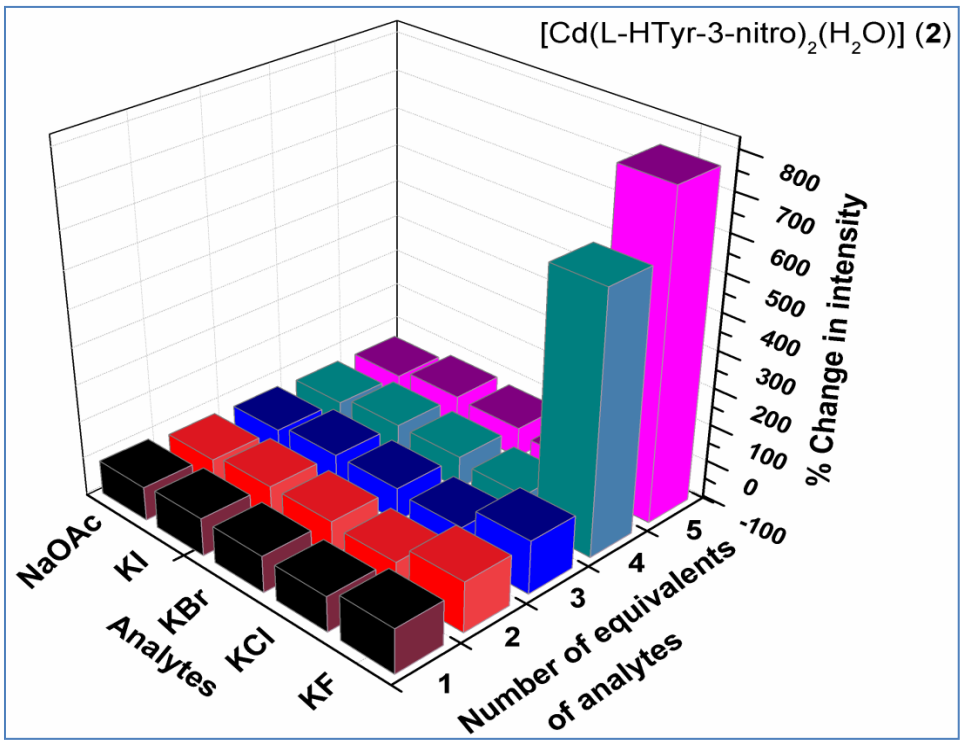

Figure 42. Representation of anion sensing ability of **2** (λ_{exc} = 220 nm , λ_{em} = 364 nm).

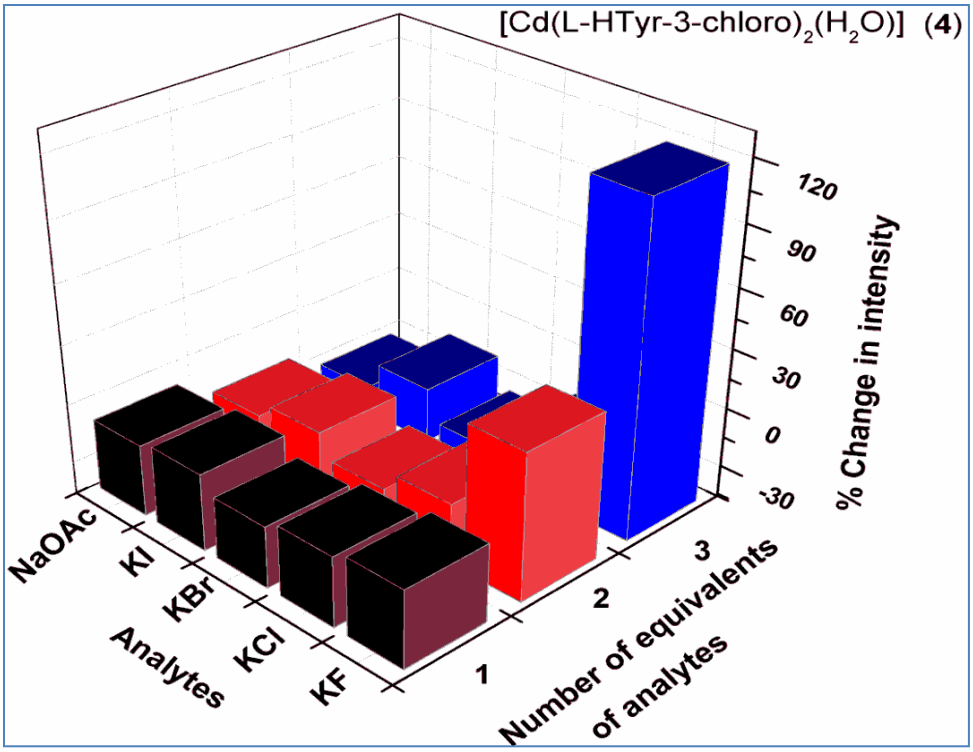

Figure 43. Representation of anion sensing ability of **4** (λ_{exc} = 220 nm , λ_{em} = 364 nm).

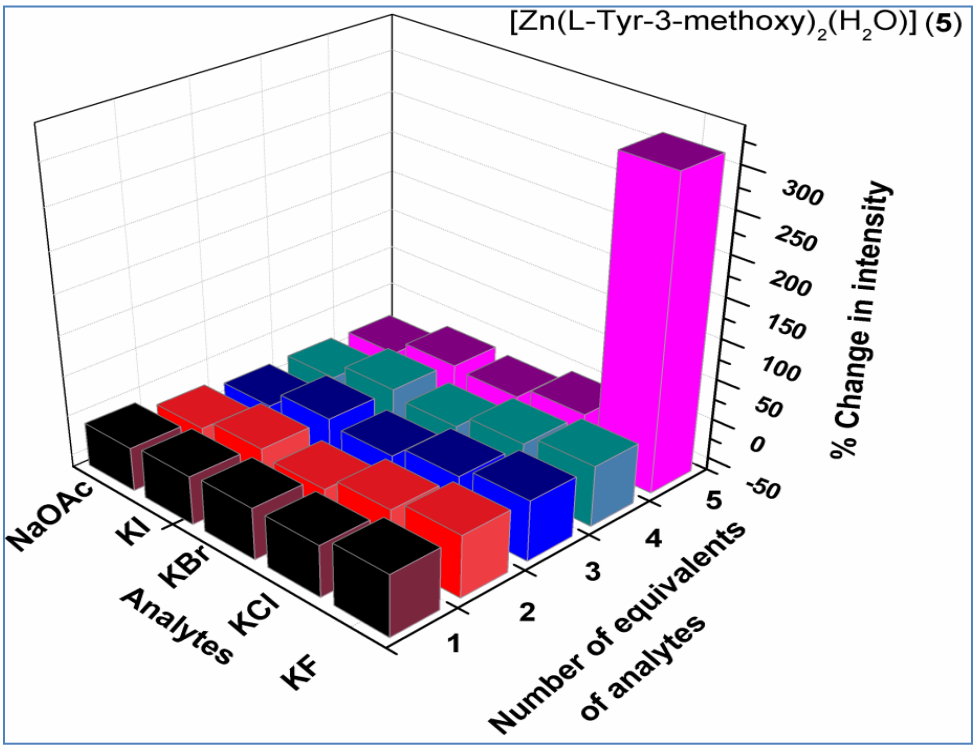

Figure 44. Representation of anion sensing ability of **5** (λ_{exc} = 220 nm , λ_{em} = 364 nm).

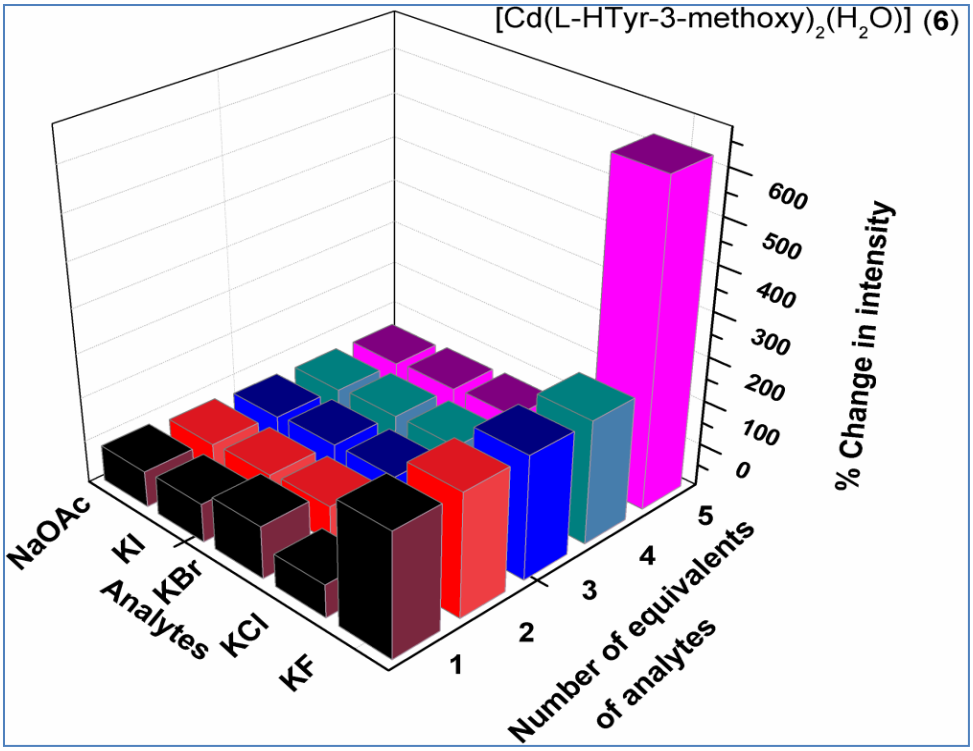

Figure 45. Representation of anion sensing ability of **6** (λ_{exc} = 220 nm , λ_{em} = 364 nm).

Chapter IV

Conclusions and Future Directions

Three new chiral ligands based on L-Tyrosine and their Zn (II) and Cd (II) complexes were synthesized in excellent yields and characterized by various analytical techniques. Fluorescence spectroscopy is used to analyze the anion sensing abilities of the ligands and their metal complexes. Ligands show differential anion sensing ability due to the solvent effect, i.e., selective sensing of fluoride in DMSO and of iodide in methanol. Metal complexes show fluoride sensing in DMSO. Cd(II) analogues show better anion sensing ability compared to the Zn(II) analogues. For the ligands as well as the metal complexes, a nitro group in the benzene ring provides better sensing ability than a chloro or a methoxy group. This fact can be attributed to the electron withdrawing ability of nitro group and thus enhancement in the anion–π interaction leading to better anion sensing ability.

In order to understand the interactions involved in the sensing study of fluoride and iodide demonstrated in this work, crystal structures of all ligands and their metal complexes as well as the fluoride and iodide adducts should be determined. Additionally, ESI-MS experiments to identify the nature of adducts can provide further evidence for such interactions studied by Fluorescence spectroscopy.

References

1. Valeur, B.; Berberan-Santos, M. N. *J. Chem. Educ.* **2011**, *88*, 731.
2. (a) Martinez-Manez, R.; Sancen, F. *Chem. Rev.* **2003**, *103*, 4419; (b) Gunnlaugsson, T.; Glynn, M.; Tocci, G. M.; Kruger, P. E.; Pfeffer, F. M. *Coord. Chem. Rev.* **2006**, *250*, 3094.
3. (a) Lan, T.; Furuyab, K.; Lu, Y. *Chem. Commun.* **2010**, *46*, 3896; (b) Ramesh G. V.; Radhakrishnan, T. P. *ACS Appl. Mater. Interfaces* **2011**, *3*, 988; (c) Mahapatra, A. K.; Maji, R.; Maiti, K.; Adhikari, S. S.; Mukhopadhyaya, C. D.; Mandal, D. *Analyst* **2014**, *139*, 309; (d) Wang, G. Y.; Yang, L. L.; Li, Y.; Song, H.; Ruan, W. J.; Chang, Z.; Bu, X. H. *Dalton Trans.* **2013**, *42*, 12865; (e) Jiang, B. P.; Guo, D. S.; Liu, Y. *J. Org. Chem.* **2011**, 76, 6101.
4. Joseph R. Lakowicz, Principles of Fluorescence Spectroscopy, 3rd edition Springer, 2006.
5. Lee, J. Y.; Farha, O. K.; Roberts, J.; Scheidt, K. A.; Nguyen, S. T.; Hupp, J. T. *Chem. Soc. Rev.* **2009**, *38*, 1450.
6. Huheey, James E., Ellen A. Keiter, and Richard L. Keiter. "Coordination Chemistry: Bonding, Spectra, and Magnetism." Inorganic Chemistry: Principles of Structure and Reactivity. New York, NY: HarperCollins College, 1993. 455-59.
7. Pure and Applied Chemistry, Volume 68, Issue 12, Pages 2223–2286.
8. Duke, R. M.; Veale, E. B.; Pfeffer, F. M.; Krugerc, P. E.; Gunnlaugsson, T. *Chem. Soc. Rev.* **2010**, *39*, 3936.
9. Ema, T.; Okuda, K.; Watanabe, S.; Yamasaki, T.; Minami, T.; Esipenko, N. A.; Anzenbacher, P. Jr. *Org. Lett.* **2014**, *16*, 1302.
10. Kumar, N; Khullar, S.; Mandal, S. K. *Dalton Trans.*, **2015**, *44*, 1520.
11. Schottel, L. B.; Chifotides, T.H.; Dunbar, R.K. *Chem. Soc. Rev.*, **2008**, *37*, 68.
12. (a) Ballester, P. *Struct. Bonding **2008**, 129*, 127 (b) Quinonero, D.; Garau, C.; Rotger, C, Frontera, A.; Ballester, P.; Costa, A.; Deya, P. M. *Angew. Chem., Int. Ed.* **2002**, *41*, 3389 (c) Quinonero, D.; Garau, C.; A. Frontera, Ballester, P.; Costa. A.; P. M. Deya. *Chem. Phys. Lett.* **2002**, *359*, 486 (c) Mascal, M.; Armstrong, A.; Bartberger, M. D. *J. Am. Chem. Soc.* **2002**, *124*, 6274 (d) Alkorta, I.; Rozas, I.; Elguero, J.; *J. Am. Chem. Soc.* **2002**, *124*, 8593 (e) Schottel, B. L.; Chifotides, H. T.; Dunbar, K. R.; *Chem. Soc. Rev.*

2008, *37*, 68 (f) Gamez, P.; Mooibroek, T. J. ; Teat, S. J.; Reedijk, J. *Acc. Chem. Res*. **2007**, *40*, 435 (g) Domasevitch, K. V.; Gural'skiy, I. A.; Solntsev, P. V.; Rusanov, E. B.; Krautscheid, H.; Howard J. A. K.; Chernega, A. N. *Dalton Trans*. **2007**, 3140 (h) Gural'skiy, I. A.; Solntsev, P. V.; Krautscheid, H.; Domasevitch, K. V. *Chem. Commun*. **2006**, 4808 (i) Schottel, B. L.; Chifotides, H. T.; Shatruk, M.; Chouai, A.; Perez, L. M.; Bacsa, J.; Dunbar, K. R. *J. Am. Chem. Soc*. **2006**, *128*, 5895.

13. Chifotides, T. H.; Dunbar, R. K. *Acc. Chem. Res.* **2013**, *46*, 894.
14. Nakamoto, K. *Infrared Spectra of Inorganic and Coordination Compounds Part B;* John Wiley & Sons, Ltd.:2009.